

Investigation of Vortex Induced Vibrations on Wind Turbine Towers

Dimitrios Livanos

October 29, 2018

Investigation of Vortex Induced Vibrations on Wind Turbine Towers

Master of Science Thesis

Author: Dimitrios Livanos

Committee:

Prof.dr. A. Metrikine	TU Delft - Chairman
Dr. Ir. H. Hendrikse	TU Delft
Dr. Ir. K.N. van Dalen	TU Delft
Dr. F. Pisanó	TU Delft
Ir. P. van der Male	TU Delft
Dr. Ing. M. Seidel	Siemens Gamesa Renewable Energy
Ir. F. Wenneker	Siemens Gamesa Renewable Energy

October 29, 2018

Summary

Vortex Induced Vibrations (VIV) is a well-known and explored topic. It is a quite complex phenomenon as it is part of different disciplines including fluid mechanics, structural mechanics, vibrations and computational dynamics. It can be found in many engineering applications such as bridges, industrial chimneys, transmission lines, marine risers in petroleum production and in other hydrodynamics applications. Despite it is a well-known and widely explored topic, the modelling of vortex induced vibrations for engineering purposes still presents a lot of issues due to the complexity of the phenomena involved. These oscillations are of great interest for structural engineers, not only because of the large oscillation amplitude but also due to the long term cyclic loads which can cause significant fatigue damage to the wind turbine towers.

In this thesis the phenomenon of VIV on wind turbine towers is examined. Before the commissioning of the towers in the offshore wind farms, there is a number of different load cases when these structures are susceptible to VIV. These cases are summarized in the following: (i) towers standing on the quay-side, (ii) on the vessel during their transportation offshore and (iii) as installed towers on the foundation (e.g. monopile or jacket) before the installation of the rotor-nacelle assembly (RNA). The main objective is to formulate a realistic model for the prediction of wind turbine towers response due to VIV. The tower geometry includes a tapered section at the top of the structure complicating the phenomenon. The thesis approach starts with a literature study and continues with investigating the different approaches proposed from the Standards (e.g. Eurocode) and the researchers over the years. Investigation of the theoretical background of each analytical model, sensitivity analysis of the main influencing parameters and comparison of the computed vibration amplitudes contributed to the identification of advantages and limitations of these approaches.

Consequently, knowledge gained from this research and data extracted from forced oscillation experiments performed in a wind tunnel contributed to the de-

velopment of a more accurate, reliable and realistic model for the prediction of the tower response due to VIV. The recommended design procedure models the fluid structure interaction through a negative aerodynamic damping and takes into account the tapered section of the tower, the effect of turbulence intensity and the shear exponent factor of the wind. Finally, fatigue analysis of the wind turbine towers is performed in order to assess the effect of VIV on the lifetime of these structures.

Concluding, through the literature study and the review of the approaches proposed by the design codes and various researchers, a design procedure for the prediction of the tower response over a range of wind velocities is developed. Simplifications of existing methodologies proposed by the Standards limit their accuracy for design purposes. Finally, further experimental investigations and CFD simulations regarding the effect of group arrangements of the towers and the effectiveness of suppression measures are proposed for future research.

Acknowledgements

I would like to express my gratitude to everyone who supported me during the whole duration of my thesis. First of all, I want to thank my committee for the selection of this challenging topic and their guidance to achieve this rewarding result.

Regarding my colleagues in Siemens Gamesa, I want to thank them for their warm welcome and their willingness to share with me their knowledge and experience. First of all, I want to thank Frits who was always available for a meeting or a chat by his desk, supporting and motivating me during this thesis. In addition, meetings with Marc were always productive and challenging and his passion about the topic pushed me every time to set the bar higher. Pim and Hayo as my university supervisors, thanks for your support and the time you dedicated to my thesis. Andrei your level of expertise on the topic and our meetings were of significant importance for the final result.

Also I want to thank my co-students at Siemens Gamesa, Irene, Fanis, Matteo, Adriaan, Max, Claudio, Jean-Luc and Landry for the great time with had together in the office.

Finally, most of all special gratitude to Nefeli who supported me continuously during this long experience in the Netherlands. Last but not least, special thanks go to my parents, my brother and sister and of course my friends for their support from distance.

Dimitrios Livanos
Den Haag, October 2018

Contents

Summary	i
Acknowledgements	iii
1 Introduction	1
1.1 General Background	1
1.2 Problem statement	2
1.3 Aim of thesis	3
1.4 Research methodology	4
1.5 Organization of Thesis	5
2 Theoretical Background	7
2.1 Basic Phenomena of Vortex Induced Vibrations	7
2.1.1 Flow around a Stationary cylinder	7
2.2 Experimental Observations	11
2.2.1 Cylinder motion and wake interference	11
2.2.2 Lock-in	12
2.2.3 Free Oscillation experiments	14
2.2.4 Forced Oscillation experiments	15
2.3 Mitigation measures	17
3 Resonance model	21
3.1 Effective Correlation Length method	21
3.1.1 Theoretical Background	21
3.1.2 Model formulation	23
3.1.3 Derivation of Resonance model	25
3.1.4 Clobe's extension	28

4 Spectral models	31
4.1 Vickery & Basu model	31
4.1.1 Theoretical background	32
4.2 Damping-Modified Spectral method	37
4.2.1 Wind tunnel tests	38
4.2.2 Aerodynamic parameter K_a	41
4.3 Model formulation	44
5 Study case of Vortex Induced Vibrations on wind turbine towers	49
5.1 Study case	49
5.1.1 Structural modeling	49
5.1.2 Wind characteristics	51
5.1.3 Aerodynamic damping ζ_a	53
5.2 Parametric study	59
6 Fatigue	65
6.1 Fatigue assessment	65
7 Conclusions	73
7.1 Conclusions	73
7.2 Recommendations for future work	75
A Appendix	77
Bibliography	79

Chapter 1

Introduction

1.1 General Background

Since ancient times, the phenomenon of Vortex Induced Vibrations (VIV) has been experienced and has been known. Ancient Greeks knew that the strings on their Aeolian harps (named after Aeolus, the Greek god of winds), when subjected to certain wind velocity would experience vibrations producing acoustical tones. The phenomenon was also documented in rabbinic records, where King David hung his kinnor (kithara) over his bed at night, where it sounded the arrival of midnight breeze [9]. In 1878, Strouhal [55] studied the vibrations caused by periodic lift forces which are associated with vortex shedding. Von Kármán, in 1912 [69], noted the stable street of alternating vortices in the wake following Benard who, in 1908, related the wake's periodicity with the vortices.

Afterwards, the Kármán Vortex street in the wake of a cylinder is a well-known and explored topic. It is quite a complex phenomenon which is part of different disciplines, including fluid mechanics, structural mechanics, vibrations, computational fluid dynamics. The subject of VIV can be found in many engineering applications, such as bridges, industrial chimneys, transmission lines, marine risers in petroleum production and in other hydrodynamic applications. Despite it is a well-known and widely explored topic, the modelling of vortex induced vibrations for engineering purposes still presents a lot of issues due to the complexity of the phenomena involved. These oscillations are of great interest for structural engineers, not only because of the large oscillation amplitude but also due to the long term cyclic loads which can cause significant fatigue damage to the structural members.

1.2 Problem statement

In the Offshore Wind industry, the risk of Vortex Induced Vibrations becomes more important as the size of the towers is increasing. It is a phenomenon of significant importance due to the fatigue damage on the wind turbine towers. The possible reduction of their lifetime can be critical for the fatigue design. Furthermore, maximum loads due to VIV events can be crucial for the design of the design of the quay side foundation frames and the sea fastenings.

Before the commissioning of the towers in the offshore wind farms, there are number of different load cases when these structures are susceptible to VIV. These cases are summarized in the following: (i) towers standing on the quay-side, (ii) on the vessel during their transportation offshore and (iii) as installed towers on the foundation (e.g. monopile or jacket) before the installation of the rotor-nacelle assembly (RNA). In the second case, critical is the period when the vessel is jacked up and there is no disturbance from its motion or the wave loads. In the third case, the time window is short and after the installation of the RNA, the additional mass is a very beneficial factor against VIV. However, in the first case, the towers may stand on the harbor for a long period of time, increasing the possibility of a VIV “event”.

Literature on Vortex Induced Vibrations on industrial concrete or steel chimneys can be directly related to the case of wind turbine towers. Since the 1960s, extensive research has been done on this phenomenon regarding the cases of industrial chimneys or television towers. The biggest difference with the wind turbine towers is the amount of structures. In case of a chimney, mitigation measures can significantly reduce the vibration amplitude. In the case of multiple towers, the effect of VIV can be more destructive due to group effects and the chosen solutions should be economical and feasible for the whole project. For example, in 1965 [49] three cooling towers, part of a group of eight, collapsed after an hour in Ferrybridge (see Figure 1.1). A witness described their motion as this of a belly dancer.

Finally, the biggest challenge for the prediction of the VIV on towers is the calculation of the maximum expected amplitude due to the various approaches of the code provisions (Eurocode, DNV, CICIND model code). More precisely, Eurocode proposes two completely different approaches for the calculation of the amplitude resulting to significantly different deflections of the tower. Furthermore, other approaches, such as DNV, CICIND model codes, result from different research perspectives. These approaches predict vibration amplitudes which in some cases differ by a factor of three or greater. Thus, the selection of the most reliable and “suitable” method for the wind turbine towers is a challenge, considering also the tapered section at the top of the structure.



Figure 1.1: Three collapsed towers in Ferrybridge, UK [49]

1.3 Aim of thesis

This thesis is firstly aiming to scrutinize the existing analysis methods described in standards, including recent advances from the literature. Through a sensitivity analysis of the methods, the main influencing parameters of VIV will be identified and mitigation measures can be pinpointed through that process. The ultimate goal of this MSc thesis project is the development of an improved and reliable model for the prediction of the Vortex Induced Vibrations on towers. The biggest challenge of the project is the development of a trustworthy model describing sufficiently such a complex phenomenon, which can be finally used in industry. Simplifications made on models proposed in the standards will be disregarded, aiming for more precise results. In the improved model, simplifications on the design rules regarding a single critical wind velocity for the tapered tower will be avoided. Aiming for more accurate estimation of the fatigue damage on the tower, the final model should include the implementation of realistic wind profiles and provide information about the dependence of the VIV amplitude on the wind velocity on site.

The availability of experimental results will contribute to the comparison/validation of the methods and the identification of their limitations.

The goals of this thesis can be summarized in the following:

- Acquire awareness and in-depth knowledge of the Vortex Induced Vibration phenomena through an extensive literature review.
- Perform a critical review on the available methods, design rules and guidelines.

- Identify the main influencing parameters of the phenomenon performing a sensitivity analysis.
- Development of an improved, reliable and trustworthy model for the prediction of VIV events and the maximum vibration amplitude on wind turbine towers. Application of realistic wind profiles covering a range of wind velocities will ensure the reliability of the developed design model.
- Estimation of the fatigue damage on the structure resulting from the selected models and identification of parameters influence on the fatigue lifetime.

1.4 Research methodology

Even if VIV phenomenon has been studied for many decades by the researchers there is no certain solution to the problem or an analytical model that can describe it sufficiently, due to the uncertainty of the various input parameters.

In the past, a lot of experiments on VIV have been performed in water in order to examine the phenomenon experienced by marine risers in the offshore oil and gas industry. Experiments in the air have been done, originated mainly from the industrial chimneys which experience VIV even at low wind velocities. Scruton (1964) [52] was one of the first researchers who examined VIV of structures and experimented on mitigation measures in order to reduced the response amplitude [53]. Furthermore, the contribution of Vickery, firstly with Watkins (1962) [68] and later on with Clark (1972) [67] and Barry [66], was of significant importance for understanding the nature of flow-induced vibrations either in-air or in-water. Finally, in 1983 in collaboration with Basu [64], [65] presented a mathematical model for predicting the across-wind response of circular cylinders. This will become the reference spectral model for many researchers in the next decades. Another researcher with important contribution is Ruscheweyh. He started his research in the seventies (see [26], [41], [42], [46], [44], [45]) and his publications on the topic continue until today. He focused mainly on the response of industrial chimneys and was one of the first to perform experiments for the case of interference galloping (group of structures). The models developed by Ruscheweyh and Vickery are the two models proposed by Eurocode [4] for the prediction of the response due to VIV. Concluding, recent publications that provide a critical review on the phenomenon can be found from Sarpkaya [47] and Williamson [70].

In recent years, with the development of wind farms and especially in the offshore industry, VIV has become a problem for the wind turbine towers. The approach selected in this thesis to examine the phenomenon of Vortex Induced Vibrations is

following. At the early stages, a detailed literature study will be carried out in order to identify the main researchers, experimental approaches and derived analytical model proposed over the years. It is of significant importance to distinguish the different experimental approaches and identify their limitations and advantages. The scope of the literature review is to gain an insight, spherical knowledge and understanding of this phenomenon.

Afterwards, having obtained a solid base and awareness of VIV, comparison of different approaches from the standards and code provisions (DNV, Eurocode, CI-CIND model code) will follow. In general, these approaches are simplifications/codified versions of complex models proposed by researchers over the years, derived either from experimental results or empirically by observed/measured responses of steel or concrete towers. In this thesis, the derivation of these simplified models from the original proposals will contribute to approach the phenomenon from a solid base. Modifications will follow in order to “adjust” these models in the case of wind turbine towers considering the tapered section at the top. Implementation of these models, taking into account realistic wind profiles for a range of wind velocities will provide information for the dependence of VIV phenomenon on wind velocity, shear factor and turbulence intensity. For this cause, a finite element model of the tower will be created in order to apply the various approaches. Through the implementation of the models, the importance of VIV on the FLS (Fatigue Limit State) and ULS (Ultimate Limit State) design will be assessed. Sensitivity analysis of the input parameters of the models will contribute to the better understanding of the phenomenon, identification of their drawbacks, simplifications, limitations, differences and examine their robustness.

Finally, experimental results provided by Lupi, already published (see [32], [30] and [33]), will be processed in order to create a model for the prediction of the tower response due to VIV. This can only be achieved through the knowledge and experience gained from the above-mentioned methodology.

1.5 Organization of Thesis

Following the Introduction, the contents of this thesis are divided in the following Chapters:

- Chapter 2 presents a brief theoretical background on the flow around a cylinder. In addition, a literature review including the main observations made through experiments is following in order to explain the “lock-in” phenomenon and the differences between free and forced oscillation experiments.

- Chapter 3 provides a brief theoretical background and description of the first approach of the Eurocode (Resonance model). Extensions performed on this model will follow and will be commented.
- Chapter 4 is dedicated on the presentation and explanation of the theory behind the Spectral models. Vickery & Basu model is followed by the Damping Modified Spectral Method (DMSM) presented by Lupi. Afterwards, process of Lupi's experimental results is performed from a different perspective, considering also the tapered section of the wind turbine towers. The results are explained and compared with relevant graphs found in the literature. Subsequently, formulation for the implementation of the spectral models is presented.
- Chapter 5 provides a detailed application of the selected, previously presented, models on a wind turbine tower. Intermediate results and graphs provide explanation of the methodologies presented in Chapters 3 and 4. Finally, sensitivity analysis is performed for the most influencing input parameters of the selected models and the results are commented.
- Chapter 6 follows the results produced in Chapter 5, presenting fatigue assessment on the wind turbine tower, computed according to selected spectral models. Afterwards, comments regarding the fatigue damage on the structure and the methodology followed are presented.
- Chapter 7 addresses the conclusions of this thesis, summarizing the main findings and contributions. Recommendations on future research are concluding this thesis.

Chapter 2

Theoretical Background

In this Chapter, a description of the Vortex-Induced Vibration phenomenon is presented, along with a brief literature review of the experimental approaches. The non-dimensional parameters that govern the flow over a cylinder are also introduced at the beginning of this chapter. Finally, a concise presentation of possible mitigation measures against VIV is concluding this Chapter.

2.1 Basic Phenomena of Vortex Induced Vibrations

2.1.1 Flow around a Stationary cylinder

VIV is a fluid-structure interaction phenomenon, which may occur when a bluff structure is placed in a flowing fluid. The fluid pressure fluctuates as vortices are shed alternately from each side of the structure. The repeating pattern of swirling vortices is responsible for the unsteady separation of fluid flow and is known as the von Kármán vortex street. The alternating shedding causes an oscillating lift and drag forces on the circular cylinder.



Figure 2.1: Visualization of the vortex street behind a circular cylinder in air [1]

When one looks closer to the boundary layer of a cylinder, the mechanism which creates shedding vortices can be explained. At the cylinder surface, there is friction due to the air viscosity. The region around the cylinder can be classified in two regions, (i) in which the flow is attached and (ii) in which the flow is separated from the cylinder surface (see Figure 2.2). At the boundary layer, the flow velocity is zero and increases to the flow velocity at the outer edge of the boundary layer. The friction of the boundary layer causes the flow to “roll-over”, creating a vortex (see Figure 2.3).

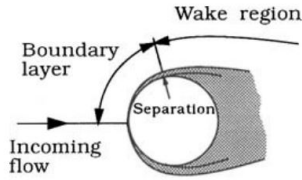


Figure 2.2: Wake and boundary layer [57]

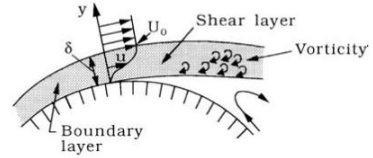


Figure 2.3: Velocity distribution and vorticity in the boundary layer [57]

This phenomenon, was firstly described by Strouhal in 1878 [55], while investigating the aeolian sound generated by wires experiencing vortex shedding. The frequency of the vortex shedding is described by the dimensionless number S_t which is defined by equation 2.1.

$$S_t = \frac{f_{st}D}{V} \quad (2.1)$$

$$V_{cr} = \frac{f_n D}{S_t} \quad (2.2)$$

$$Re = \frac{VD}{\nu} \quad (2.3)$$

where f_{st} is the frequency of the vortex shedding (Strouhal frequency), D the characteristic length of the cross section and V the free stream flow velocity. Experimental results show that across-flow oscillations occur at the shedding frequency, while in-line oscillations occur at twice the shedding frequency. In order to define the flow velocity in which resonance occurs, one has to replace the shedding frequency with the natural frequency of the structure in equation 2.1. Consequently, equation 2.2 is obtained, describing the critical wind velocity V_{cr} .

Vortex shedding is a function of the Reynolds number, equation 2.3. Lienhard [29] summarized the major regimes of fluid flow across circular cylinders depending on the Re . It evolves from the regime of unseparated flow ($Re < 5$) to the re-establishment of the turbulent vortex street ($Re > 3.5 \cdot 10^6$), where we can no longer speak of the eddy-shedding frequency, but only report the dominant one

in a frequency spectrum. Strouhal number depends on the body shape and also on the Reynolds number. The relationship between Strouhal and Reynolds number is presented in Figure 2.4. As the figure indicates $S_t \simeq 0.2$ in the subcritical range ($Re = 500 \sim 10^5$), almost constant. However, in the transcritical range ($Re = 10^5 \sim 10^6$), its value increases and there is also an upper and lower branch, indicating the difference between a cylinder with rough and a smooth surface.

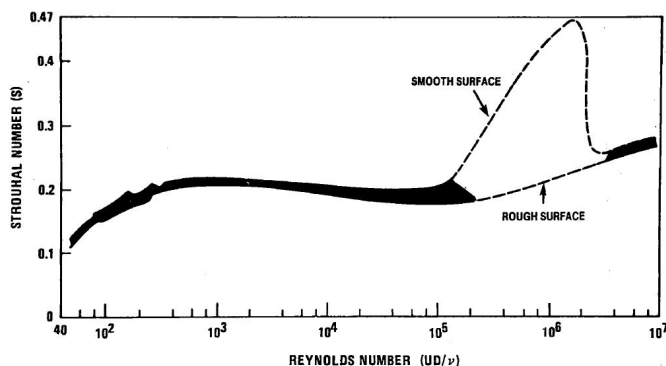


Figure 2.4: Strouhal versus Re number for circular cylinders [9]

In the following paragraphs, more fundamental parameters of the phenomenon will be presented and their effect on the vibration amplitudes will be briefly explained.

The first dimensionless parameter is the reduced velocity V_r . It is expressed as the mean velocity of the flow normalized by the oscillation frequency and the cylinder diameter. It is given by equation 2.4:

$$V_r = \frac{V}{f_n D} \quad (2.4)$$

The response amplitude of the structure is usually presented as the ratio of the displacement A_y over the diameter of the cylinder D . Thus, in the next Chapters the vibration amplitude is usually expressed as the normalized amplitude.

The oscillations due to VIV depend primarily on the reduced damping, stability parameter or Scruton number. The susceptibility of a structure to VIV highly depends on the value of this parameter, expressed as the multiplication of the ratio of structural to fluid mass by the structural damping. It is given by the following equation 2.5:

$$Sc = \frac{2\delta_s m_{i,e}}{\rho b^2} \quad (2.5)$$

where $m_{i,e}$ is the equivalent or effective mass per unit length for the mode i . Effective mass is given by equation 2.6:

$$m_{i,e} = \frac{\int_0^h [m(z)\Phi^2(z) + \sum M_j(z)\Phi(z)^2] dz}{\int_0^h \Phi^2(z) dz} \quad (2.6)$$

where $m(z)$ is the mass per unit length of the structure, M_j the concentrated point masses and Φ the mode shape.

The damping ratio of a structure is frequently expressed as the ratio of the viscous to the critical damping. It is described by equation 2.7.

$$\zeta = \frac{c}{2m\omega_n} = \frac{\delta_s}{\sqrt{(2\pi)^2 + \delta_s^2}} \quad (2.7) \quad \delta_s = \ln \frac{y_n}{y_{n+1}} \quad (2.8)$$

where c is the viscous damping coefficient, m the mass of the structure and ω_n the natural angular frequency. However, the damping value in literature is often expressed with the logarithmic decrement δ_s which is computed by the successive peaks of a free decay test. In equation 2.8, y_n and y_{n+1} are the successive peaks measured in the free decay test.

Regarding the approaching wind flow, turbulence intensity I_v and its shear in the spanwise direction of the structure are the main influencing parameters. Turbulence intensity I_v is expressed through equation 2.9:

$$I_v = \frac{\sqrt{\tilde{u}^2}}{\tilde{u}} \quad (2.9)$$

where $\sqrt{\tilde{u}^2}$ is the root-mean-square value of the wind velocity fluctuations and \tilde{u} the mean value of the velocity. The effect of turbulence is similar to the cylinder's roughness. The increase of Reynolds number due to turbulence, affects the value of S_t and this is illustrated in Figure 2.6. Considering the shear of the incoming flow, as shown in Figure 2.5, the wind velocity differs along the height resulting to different shedding frequencies f_{st} following the Strouhal relationship (see equation 2.1).

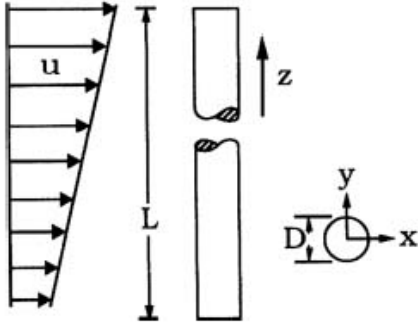


Figure 2.5: Shear in the spanwise direction of the structure [58]

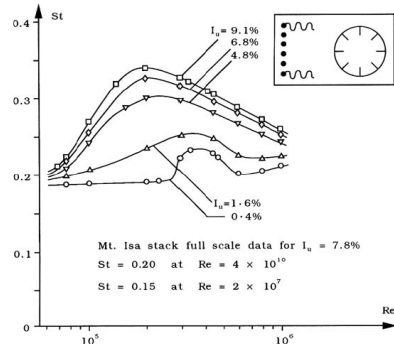


Figure 2.6: Effect of turbulence on vortex-shedding frequency through Strouhal relationship [11]

Concluding, the above mentioned parameters will play a significant role on the analytical models which are presented in the next Chapters. The ideal model should take into account their effect, representing sufficiently the physics of the VIV phenomenon.

2.2 Experimental Observations

2.2.1 Cylinder motion and wake interference

It should be mentioned that the vortex shedding frequency in equation 2.1 refers to a stationary cylinder, meaning a fixed rigid body. However, the vibration of a flexible structure induced by transverse fluid flow, continuously changes the boundary and flow conditions, generating a more complex problem due to the interaction between dynamic flow and cylinder motion. Investigations on VIV have shown that the cylinder motion primarily depends on geometry, mechanical and material damping, flow density and structural frequency.

According to Blevins [9], when the vibration frequency is close or equal to the shedding frequency, the cylinder motion can (i) increase the strength of the vortices ([15], [24]), (ii) increase the spanwise correlation length of the wake ([60], [36], [18]), (iii) dictate the shedding frequency causing its synchronization with the frequency of the vibrating cylinder (referred as “lock-in” or “synchronization” effect)

([5]), (iv) increase the coefficient of the drag force and finally ([48], [59], [8]), (v) change the phase, pattern and sequence of the vortices ([71],[73], [37]).

Cylinder vibration interferes with the wake, especially when the vibration frequency is close to the shedding one. A cylinder experiencing VIV interferes with the shear layers leading to vortex shedding. Subsequently, alternating forces in transverse and in-line direction are created resulting to structure's motion. Finally, this results to common vibration and shedding frequency, as the vibration dictates the shedding frequency. The correlation of the vortex shedding along the cylinder, which is a measure of the three-dimensionality of the wake, is increased due to the motion, amplifying the aforementioned phenomena. Therefore, cylinder motion is becoming part of this instability and serves as a magnifier, organizer and synchronizer of the phenomenon [47].

Moreover, cylinder motion influences the pattern and the phase of the vortices. It has been observed that the vortex is shed from the opposite side of the maximum displacement, when the vibration is lower than the shedding frequency. However, when the cylinder is vibrating at a frequency higher than the shedding one, the vortices tend to shed from the same side of the maximum displacement. Thus, a phase shift of 180 degrees happens between shedding and cylinder motion.

2.2.2 Lock-in

In general, "lock-in", is referred in the literature the phenomenon when the wake synchronizes with the motion of the structure. In the lock-in range, resonant oscillations happen and substantial energy is transferred to the structure from the wake, resulting to large vibration amplitudes. It is usually defined as $f_{vib}/f_s \simeq 1$, where f_{vib} is defined the oscillation frequency and f_s the vortex shedding frequency. As the flow velocity is changing (increasing or decreasing) and the vortex shedding frequency f_{st} approaching the oscillation frequency f_{vib} , f_{st} locks-into the latter one. For a range of flow velocities, cylinder's vibration dictates the shedding frequency, violating the Strouhal relationship which is no longer valid in the "lock-in" regime (see Figure 2.7).

It is important to note that perfect synchronization should not be expected as the cylinder is continuously interacting with the fluctuations of amplitude, correlation-length, phase angle, separation point and flow velocity. However, experiments performed in air channel have shown more "stable" synchronization phase than experiments in water, resulting from the much higher mass ratio of the vibrating cylinder and the fluid. Therefore, in air, the resultant vibrations occur at or very close the natural frequency f_n of the system, meaning $f_s \simeq f_n$. "Lock-in" is visualized in Fig-

ure 2.7, presented by Feng [19] who performed free-oscillation experiments in air channel.

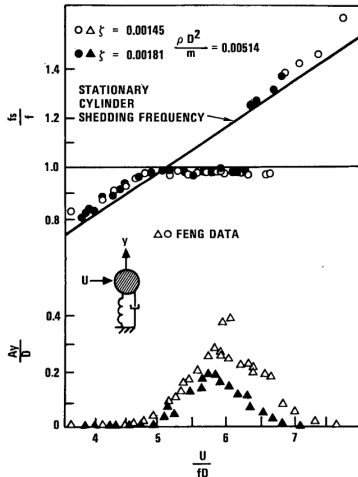


Figure 2.7: Oscillation phenomena of a spring mounted cylinder freely oscillating in air, f is the natural frequency [19]

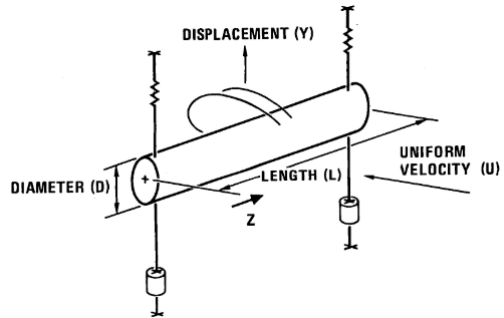


Figure 2.8: Schematic representation of experimental set-up for free vibration experiments[9]

In Figure 2.7, it can be observed that transverse oscillations occur over velocity range or $4 < V_r < 8$, where $V_r = \frac{V}{fD}$ is the reduced (normalized) flow velocity.

Finally, a more accurate definition of “lock-in” is the phenomenon when the shedding frequency f_{st} violates the Strouhal relationship and becomes equal to the natural frequency of the system f_n . On the other hand, “synchronization” is the phenomenon when the shedding frequency f_s violates the Strouhal relationship and matches another frequency (common frequency f_{com}), which is not necessarily the natural frequency. It becomes clear that “lock-in” is a specific case of the “synchronization”. In VIV phenomena happening in water, the added mass (or added stiffness) changes the natural frequency of the structure (such as risers) resulting to vibration in different frequency. This is called “synchronization” as the natural frequency differs from the vibration frequency ($f_n \neq f_{vib}$ and $f_{vib} = f_{com} = f_{st}$).

In the past fifty years, major research has been done on the understanding of the VIV phenomenon. The research mainly involves two different approaches, the free and the forced oscillation experiments. Aim of these tests is the understanding

of different aspects of VIV, such as “lock-in”, wake formation, “hysteresis” effect, extract lift and drag or added-mass and added-damping coefficients. In addition, most of the researchers focused on the investigation of the effect of mass-damping parameter on the response amplitude. In the next sections, a brief presentation and explanation of the main and more useful for this thesis researches, are following.

2.2.3 Free Oscillation experiments

Free vibration tests are performed either in a wind or in a water tunnel, without using any exciting mechanism for the oscillation. The cylinder is mounted on springs and dashpots (such as magnets), allowing free vibration with various damping ratios. The flow velocity increases from low values to higher ones, step by step, measuring the steady state vibration amplitude for each flow velocity. The cylinder is either rigid or flexible and moves perpendicular to the flow, as can be seen in Figure 2.8. The free oscillation of a cylinder is closer to the “true” nature of the VIV, indication that is a self-excited vibration.

In general, the free-vibration experiments reported to date, are mainly using water as the fluid medium, also for flow visualization reasons. Therefore, experiments performed in air are limited in the literature. Khalak and Williamson (1997) presented amplitude response curves for three different masses exposed to three different damping values [28]. Comparing their results with Feng’s experiments (see Figure 2.9), it can be observed that due to lower mass ratio in the case of air, the vibration amplitudes are much lower than the experiments performed in water. In addition, one can notice the wider synchronization range (V_r) of the response in water. Furthermore, in the latter one, effects such as response hysteresis (upper and lower branches) are more profound.

Feng’s [19] free oscillation experiments conducted in air have been referred extensively in the literature. These were conducted with a single degree of freedom flexible cylinder with a large mass ($m^* = \rho_m / \rho_{air} = 248$, $\zeta = 0.103\%$, $m^*\zeta = 0.255$) and large Re which varies with V_r from 10^4 to $5 \cdot 10^4$. Later on, researchers based their experiments on Feng’s data in order to explore and answer new questions for the VIV phenomenon or to validate their findings.

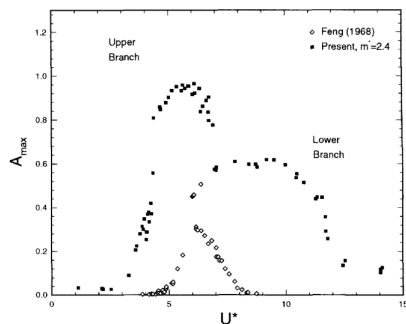


Figure 2.9: Comparison between Feng's and Khalak's experimental results of free vibration tests conducted in air ($m^* = 2.4$) and water ($m^* = 248$) respectively [28]

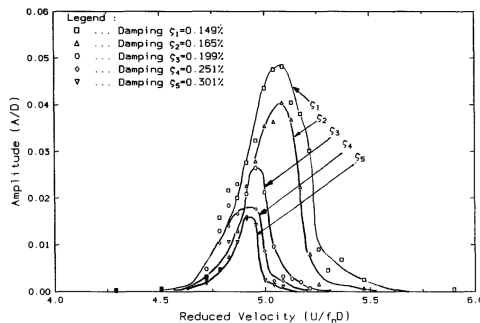


Figure 2.10: Normalized vibration amplitude versus reduced velocity for various values of mechanical damping [21].

Later on, a set of free oscillation experiments were conducted in air by Goswami [21] in order to develop a mathematical (analytical) model for the calculation of the maximum vibration amplitude [22]. In this research, influence of mechanical damping, up-stream turbulence and spanwise correlation of shedding were examined. A rigid cylinder was mounted in springs ($k = 4.1 \text{ N/mm}$) and circular plates ($d = 254 \text{ mm}$) were used to eliminate the near end effects. The damping was adjusted electromagnetically and varied from $\zeta = 0.149 \%$ to $\zeta = 0.301 \%$. In Figure 2.10 the vibration amplitude versus the reduced velocity V_r , for various values of mechanical damping is presented. One can notice the reduction of the synchronization range (narrower range of V_r) and the vibration amplitude for increasing values of mechanical damping. The amplitude is lower than this in Feng's experiments as the Scruton number is considerable higher in the former case.

Earlier than Feng (1968), Vickery and Watkins (1962) investigated the effect of damping on the response of cylindrical cantilevers of circular cross section, performing experiments both in water and in air [68]. Later on Scruton [50], presented some of the results of the aforementioned research, illustrating the response amplitude for three different damping values.

2.2.4 Forced Oscillation experiments

Forced oscillation experiments are performed using an excitation mechanism. The flow velocity is kept constant while the amplitude and frequency of oscillation vary.

These tests can regularize and idealize the various aspects of VIV, leading to extraction of forces from repeated sinusoidal oscillations. At each test, the required driving force for the oscillation is measured throughout a range of reduced velocities V_r . In Figure 2.12 a test section for performing forced oscillation tests is presented. The measured forces are in-phase and out-of-phase with the displacement. The first ones are usually related with the “added-mass” or “added stiffness” (water experiments) and the latter ones with the damping of the system. The difference between the force and the free oscillation experiments is, that in the first ones, the Re number is constant while in the latter ones varies. Furthermore, in free vibration there is two way coupling between the wake and the cylinder motion, which is the driven mechanism.

Bishop and Hassan [8] in 1964 investigated the lift and drag forces on an oscillating cylinder in water. Later on, Sarpkaya [48] performed measurements of forces on a rigid cylinder vibrating in water, extracting added-mass coefficients. These results were used for the prediction of the response of a freely oscillating mounted cylinder. Afterwards, Carberry [10] in 2005 examined the wake states from a circular cylinder subjected to controlled sinusoidal oscillations, observing a “transition” between “low frequency and high frequency state” [72].

In the literature, there are debates about the connection between forced and free oscillation experiments. Morse and Williamson [35] (VIV in water) demonstrated that with carefully selected conditions, the forces extracted from forced oscillation experiments can reproduce the results of free oscillation ones. Figure 2.11 illustrates the reproduction of free-vibration experiments performed by Govardhan and Williamson [23].

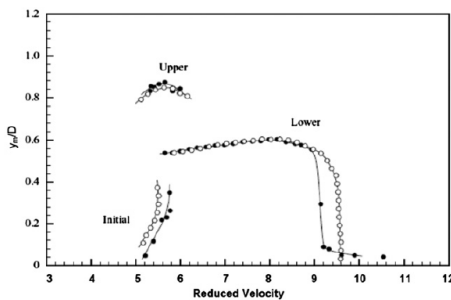


Figure 2.11: Measured response from free-vibration test [23] (●) and prediction (○) of the response by forced-vibration experiments [35]

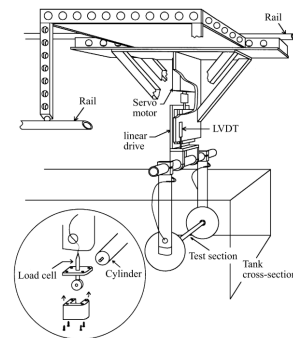


Figure 2.12: Test section for forced oscillation tests [27]

Furthermore, Hover [27] recently (1997) performed free and forced oscillation tests in a water tank extracting the amplitude and phase of the lift coefficient on both cases. The correspondence of the lifting coefficient in forced and free vibration tests was found remarkably close. However, in forced oscillation tests, the force correlation along the span of the cylinder is better. Moreover, tests performed in a tapered cylinder resulted to “lock-in” at lower reduced velocities V_r than in a uniform one. In Figures 2.13 and 2.14 the correspondence of the lift coefficient from forced and free oscillation experiments is illustrated.

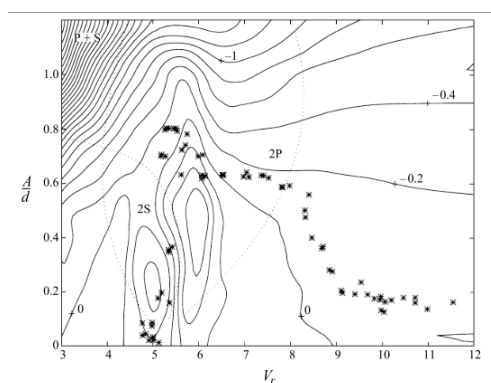


Figure 2.13: Contour plot of lift coefficient from forced oscillation tests with free oscillation data (*) [27]

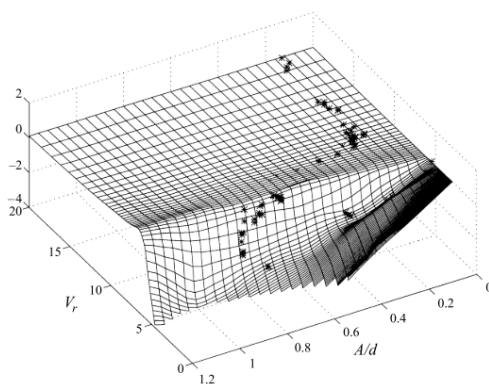


Figure 2.14: Mesh plot of lifting coefficient from forced vibration tests with data from free oscillation ones (*) [27]

2.3 Mitigation measures

The resulting amplitude from VIV can cause severe fatigue damage even collapse of the entire structure. Mitigation measures for the reduction or even elimination of the VIV response were being subject of research mainly concerning industrial chimneys. They have been researched for more than 50 years. In the next paragraphs, the main vortex suppression measures and devices are presented and commented on their effectiveness.

1. Avoid resonance adjusting natural frequency f_n

A simple way to prevent large vibration amplitudes due to VIV is by adjusting the natural frequency of the structure. Stiffening the structure, meaning higher natural frequency results to higher critical wind velocities. In this way, considering the probability of the wind velocity on site, oscillations due to VIV can be avoided. Especially in smaller structures this can be a feasible solution.

2. Increase structural damping ζ_s

In cases that the vibration amplitude is critical for the design of a structure, additional damping devices or increase of the structural damping can reduce significantly the displacement to less than 1 % of the diameter. This value corresponds to deflection which is less than that induced by drag forces. Blevins [9] proposes increase of Scruton number by either increasing structural damping or increase of the structural mass. Damping can also be increased by permitting scraping or banging between the structural elements or using materials such as rubbers and viscoelastic ones. Finally, the most commonly used damping devices in industrial chimneys are the tuned mass dampers (TMD) and the tuned liquid dampers (TLD). They are based on the counteracting inertial force created by a mass placed near the top of the tower. These are tuned to move out-of-phase with the natural frequency of the tower. In Figures 2.15 and 2.16 examples of a tuned mass and liquid dampers are presented.



Figure 2.15: Tuned mass damper of 41 tonnes installed on top of a 180m concrete chimney [2]



Figure 2.16: Liquid damper on top of a 100 m steel stack used also as a top platform [2]

3. Vortex suppression devices

These devices aim to affect the separation lines and the separation layers suppressing in this way the fluctuating forces. Scruton and Walshe [53] were the first who examined the effectiveness of helical strakes on avoiding wind-excited oscillations of cylindrical structures. The parameters that affect the effectiveness of the strakes are their height, pitch and number (see Figure 2.17). Pitch is related to the diameter of the structure, presented also as the length the strake needs to perform one turn around the cylinder. Vickery and Watkins [68] performed tests in water and found that strakes are as effective as they are in the air. Ruscheweyh [39] performed tests on the helical strakes confirming the optimal pitch of $4D$ to $5D$ covering the top third of the height. In Figure 2.18 the effect of helical strakes on the vibration amplitude is presented.

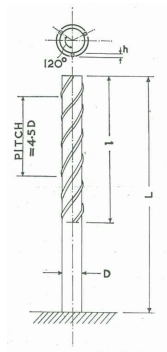


Figure 2.17: Typical arrangement of helical strakes [68]

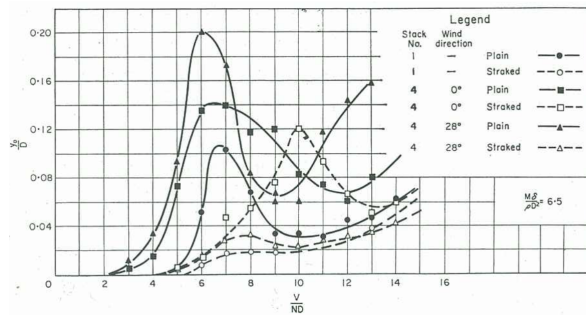


Figure 2.18: Normalized amplitude versus reduced velocity for plain and straked cylinders [68]

Concluding, there are more suppression devices such as wires, fins and studs.

More details and an extensive literature review on means for suppressing vortex shedding can be found in [73] by Zdravkovic (1981).

Chapter 3

Resonance model

In this Chapter, a description of the Effective Correlation Length method, formulated by H. Ruscheweyh, is presented. This model is the first approach, proposed by Eurocode, for the prediction of the response of structures due to VIV. Derivation of the final equation is following, aiming to disregard simplifications performed in the version of Eurocode [4].

3.1 Effective Correlation Length method

3.1.1 Theoretical Background

A complex phenomenon, like Vortex Induced Vibrations, cannot be described by a simple equation. Current codified approaches for predicting cross-wind oscillations model the fluid-structure interaction in different ways. Regarding the first approach of the Eurocode, the aeroelastic interaction is modelled through a load modification. The load correlation length is increasing with increasing amplitude of the vibration. Therefore, the model developed by Ruscheweyh is called the Effective Correlation Length Method. The increase of the correlation length of the vortex exciting force with increasing oscillation amplitude has been described by Toebe [61], Novak & Tanaka [16] and van Koten [62]. In Figure 3.1, it can be recognized that sections of the cylinder are either out-of-phase or in-phase. The average length of the in-phase sections is termed as the correlation length.

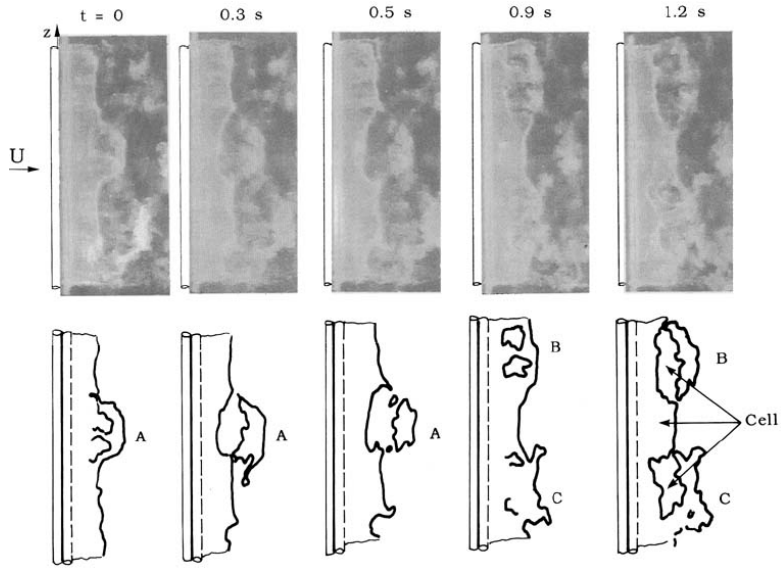


Figure 3.1: Effect of cross-flow vibration amplitude on the correlation length of a cylinder [58]

A set of experiments were performed by Novak & Tanaka [16] and the results are presented in Figure 3.2. One can observe that the correlation along the cylinder is higher when it oscillates at higher amplitudes. In addition, turbulence intensity I_v affects its value, reducing it in the case of increasing turbulence (see Figure 3.3).

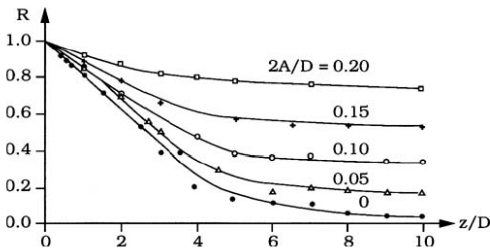


Figure 3.2: Effect of vibration amplitude (A/D) on the correlation length of a cylinder [16]

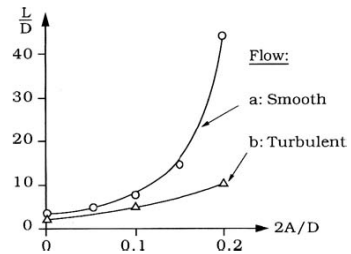


Figure 3.3: Effect of Turbulence on the correlation length [16]

3.1.2 Model formulation

The oscillation of a structure in the cross-wind direction under vortex shedding load can be described by equation 3.1. The structure is modelled as a one degree of freedom system (1 DOF), as presented in Figure 3.7.

$$\ddot{y}(t) + 2 \cdot \omega_n \cdot \zeta_n \cdot \dot{y}(t) + \omega_n^2 \cdot y(t) = \frac{F_L(t)}{M_n} \tag{3.1}$$

In this equation 3.1, the lift force F_L is applied at the correlation length L_j . According to Figure 3.4, the exponential function has been approximated by a linear and two constant parts.

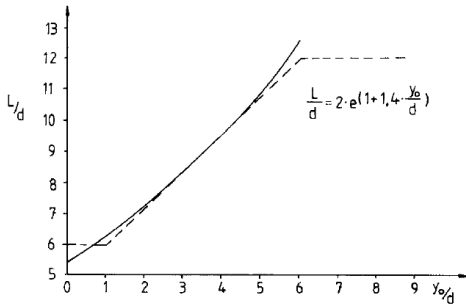


Figure 3.4: Effective correlation length ratio L/d versus peak amplitude ratio y_0/d [44]

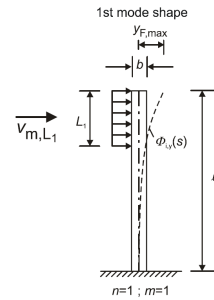


Figure 3.5: Correlation length L_j for a cantilever beam [4]

The correlation length depends on the vibration amplitude and its value is approximated as shown in Table 3.1. Firstly, a vibration amplitude is assumed to select a correlation length. Then, the lift force is applied and the computed response should match the assumed one. Thus, an iterative procedure is required for the computation of the response amplitude.

Table 3.1: Linear approximation of the effective correlation length ratio L/d [44]

L/d	y_0/d
6	≤ 0.1
$4.8 + 12y_0/d$	$0.1 < y_0/d < 0.6$
12	≥ 0.6

The model considers a harmonic lift force P_n in the resonance with the vibration mode. In order to compute the maximum vibration amplitude, equation 3.2 can be followed.

$$y_{max} = \frac{\pi}{\delta_n} \frac{P_n}{\omega_n^2 M_n} \quad (3.2)$$

The method, as presented also in the Eurocode[4], can be expressed in dimensionless terms by the following equation 3.3:

$$\frac{y_{max}}{d} = \frac{1}{Sc} \cdot \frac{1}{St^2} \cdot c_{lat} \cdot K \cdot K_w \quad (3.3)$$

where c_{lat} is the lateral force coefficient, Sc is the Scruton number (equation 2.5), St the Strouhal number (equation 2.1) given as $St = 0.18$. The coefficient K is the mode shape factor and K_w is the correlation length factor. The lateral force coefficient depends on the Reynolds number and its values are presented in Figure 3.6.

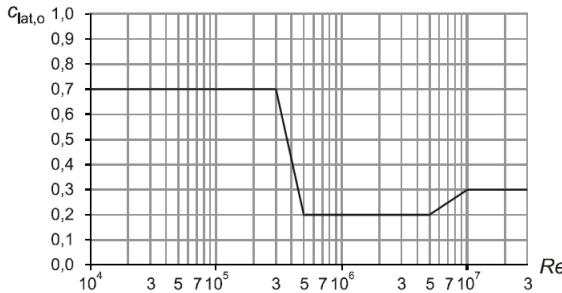


Figure 3.6: Basic value of the lateral force coefficient c_{lat} versus Reynolds number [4]

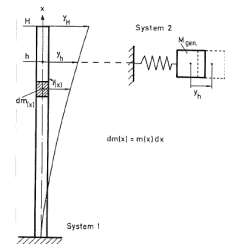


Figure 3.7: Generalization of a continuum system [40]

In the case of a cantilever beam, mode shape factor is approximated as $K = 0.13$. The coefficient K_w includes the aeroelastic effects and depends on the correlation length. Its values, from a mathematical point of view, can range from 0 to 1 but it is limited to values of $K_w \leq 0.6$. Value of $K_w = 1$ means full correlation along the height of the tower. The equations below 3.4 and 3.5 can be used for the calculation of these two factors.

$$K = \frac{\sum_{j=1}^m \int_{l_j} |\Phi_{i,y}(s)| ds}{4\pi \sum_{j=1}^m \int_{l_j} \Phi_{i,y}^2(s) ds} \quad (3.4) \quad K_w = \frac{\sum_{j=1}^n \int_{L_j} |\Phi_{i,y}(s)| ds}{\sum_{j=1}^m \int_{l_j} |\Phi_{i,y}(s)| ds} \leq 0.6 \quad (3.5)$$

where l_j is the length of the structure, L_j the correlation length computed from the table 3.1 and $\Phi_{i,y}(s)$ the mode shape of mode i .

3.1.3 Derivation of Resonance model

In this section the derivation of the final equation proposed by Eurocode (see equation 3.3) is presented. This will allow to understand the final formulation and also apply this method to towers with a tapered section. This leads to lower amplitudes of the vibration for most of the cases. Furthermore, the simplicity and limitations of the Ruscheweyh's model can be identified.

The dynamic response of a system can be computed by superimposing the response of all modes, as can be seen in equation 3.6.

$$y_{0,rms}(x) = \sum_{j=1}^n \left[\frac{b_j}{\sqrt{(1 - \eta_j^2)^2 + (2\xi_j \eta_j)^2}} \cdot \Phi_{yj}(x) \right], \quad b_j = \frac{F_j}{\omega_j^2 M_j} = \frac{F_j}{K_j} \quad (3.6)$$

where η is the ratio of the force frequency over the natural one f_n , M_j and F_j are the generalized mass and force. They can be computed from the following equation 3.7:

$$M_j = \int_0^L \mu(x) \Phi_{yj}^2(x) dx, \quad F_j = \int_0^{L_p} p_k(x) \Phi_{yj}(x) dx \quad (3.7)$$

where L_p is the effective correlation length. In VIV induced by wind flow around the structure, the vibration frequency is equal to the natural frequency of the system. According to the resonance model, the harmonic lift force is dictated by the structural motion and the shedding frequency equals the natural frequency during lock-in mode. Therefore, the ratio η is equal to one. In addition, since the force frequency is equal to the natural frequency f_n , the structure will vibrate in the first mode shape. Thus, considering $\eta = 1$ and substituting 3.7 to 3.6, equation 3.8 is derived to compute the dynamic response at the resonance point.

$$y_{0,rms}(x) = \left[\frac{\pi}{\delta} \cdot \frac{\int_0^{L_p} p_k(x) \Phi_y(x) dx}{\omega_n^2 \int_0^L \mu(x) \Phi_y^2(x) dx} \right] \cdot \Phi_y(x) \quad (3.8)$$

where $\delta = 2\pi\zeta$ is the logarithmic decrement of damping and p_k the wind pressure in the cross wind direction. The wind pressure p_k is expressed by equation 3.9.

$$p_k(x) = \frac{1}{2} \rho c_l(x) D(x) V_{cr}(x)^2 \quad (3.9)$$

where c_l is the lifting coefficient, V_{cr} the critical wind velocity and D the diameter at each level. Substituting the expression of the wind pressure, equation 3.10 is derived by equation 3.8.

$$y_{0,rms}(x) = \left[\frac{1}{2} \rho \frac{\pi}{\delta} \frac{\int_0^{L_p} c_l(x) D(x) V_{cr}(x)^2 \Phi_y(x) dx}{\omega_n^2 \int_0^L \mu(x) \Phi_y^2(x) dx} \right] \cdot \Phi_y(x) \quad (3.10)$$

The integral part at the denominator is extended as follows:

$$\int_0^L \mu(x) \Phi^2(x) dx \cdot \frac{\int_0^L \Phi^2 dx}{\int_0^L \Phi^2 dx} = M \int_0^L \Phi^2 dx \quad \text{with} \quad M = \frac{\int_0^L \mu(x) \Phi^2 dx}{\int_0^L \Phi^2 dx} \quad (3.11)$$

where M is the normalized modal mass. Substituting those to the above equation of the displacement shape $y(x)$:

$$y_{0,rms}(x) = \left[\frac{\pi}{\delta} \frac{\rho}{2} \frac{1}{4 \pi^2 f_n^2 M} \frac{\int_0^{L_p} c_l(x) D(x) V_{cr}(x)^2 \Phi_y(x) dx}{\int_0^L \Phi^2 dx} \right] \cdot \Phi(x) \quad (3.12)$$

At this stage, the varying diameter along the height can be considered. The maximum displacement at the tower top considering the tapered section of the structure is calculated by equation 3.13:

$$Y_{0,rms} = \frac{\pi}{\delta} \frac{\rho}{2} \frac{1}{4\pi^2 f^2 M} \frac{\int_0^{L_p} c_l(x) D(x) V_{cr}(x)^2 \Phi dx}{\int_0^L \Phi^2 dx} \quad (3.13)$$

The above presented equation 3.13 will be used in the next Chapters as an extended version of the Effective Correlation Length method in order to take into account the varying diameter along the height of the tapered structures. Simplification of this equation has been performed in the version of Eurocode by assuming constant diameter. Therefore, V_k , D and c_l are not functions anymore of the x position along the height and equation 3.14 is derived. The lift coefficient c_l is transformed to the rms of the lift coefficient c_{lat} . Furthermore, the peak amplitude Y_{max} is calculated by multiplying equation 3.13 with a peak factor g [43](see Figure 3.8).

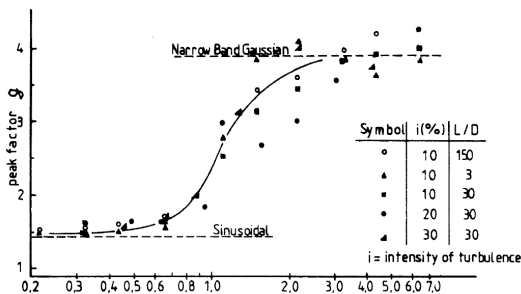


Figure 3.8: Peak factor g after Vickery & Basu [64]

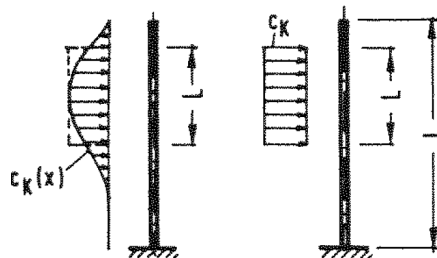


Figure 3.9: Load distribution on an oscillating cantilever beam [38]

$$Y_{max} = \frac{\pi}{\delta} \frac{\rho}{2} \frac{V_{cr}^2}{4 \pi^2 f_n^2} \frac{c_{lat} D}{M} \frac{\int_0^{L_p} \Phi dx}{\int_0^L \Phi^2 dx} \quad (3.14)$$

Introducing the Strouhal (equation 2.1) and Scruton (equation 2.5) numbers, equation 3.14 is transformed to equation 3.18.

$$\frac{Y_{max}}{D} = \frac{1}{S_t^2} \frac{1}{S_c} c_{lat} \frac{\int_0^{L_p} \Phi dx}{4\pi \int_0^L \Phi^2 dx} \quad (3.15)$$

Afterwards, the force is assumed to be applied not in the correlation length L_p but in the whole length of the structure L . The fraction of the two integrals becomes the mode shape factor K .

$$K = \frac{\int_0^L \Phi dx}{4\pi \int_0^L \Phi^2 dx} \quad (3.16)$$

However, a correlation length factor K_w is introduced to justify this simplification of the integral (see equation 3.17). The distribution of the lift force in the cross-flow direction can be observed in Figure 3.9. At the end, the load is extended to the tower top, neglecting the free end effects.

$$\int_0^{L_p} c_l(x) D(x) \Phi(x) dx = c_{lat} D \int_0^{L_p} \Phi dx = c_{lat} D K_w \int_0^L \Phi dx \quad (3.17)$$

Finally, substituting the mode shape and the correlation length factors K, K_w , the codified version proposed by Eurocode is derived:

$$\frac{Y_{max}}{D} = \frac{1}{S_t^2} \frac{1}{S_c} c_{lat} \frac{\int_0^{L_p} \Phi dx}{\int_0^L \Phi dx} \frac{\int_0^L \Phi dx}{4\pi \int_0^L \Phi^2 dx} = \frac{1}{S_t^2} \cdot \frac{1}{S_c} \cdot c_{lat} \cdot K_w \cdot K \quad (3.18)$$

Concluding, one can notice the extended simplifications performed in a model. In addition, considering that the values of the correlation length were derived empirically with lack of experimental results, it can be characterized as an empirical simple model with limitations. Nevertheless, its application over the last 30 years should not be ignored.

3.1.4 Clobes's extension

The Effective Correlation Length method, as presented from Ruscheweyh, has been used for decades for the prediction of the response due to VIV. Comparison of the predicted with the measured vibration amplitudes is, in most cases, satisfactory. However, there have been measured amplitudes which are much higher than the computed ones. Cracks have been identified in steel chimneys in Denmark, which had been designed according to this approach, after a very small number of cycles.

Clobes [13] reported this discrepancy which is visualized in Figure 3.10. One can notice the difference between the predicted and measured/observed amplitudes deriving from different models. The second approach of the Eurocode included in this graph, called the spectral method is a simplification of V&B model which is presented extensively in Chapter 4 and can be found in [4].

Clobes mentioned that most of the extreme amplitudes occurred during winter and/or in the evening/early morning. As mentioned before and presented in Figure 3.3, turbulence intensity I_v acts as a destabilizing factor of the VIV phenomenon. At the previously mentioned "extreme" occasions, its value is lower than usual and the nocturnal boundary layer is most probable to develop. This is a layer which is characterized by weaker, sporadic turbulence due to a stable stratification of the atmosphere [56]. According to Tanaka [16], in these conditions there is much higher correlation of the forces along the height of the tower. For this reason, Clobes proposed the increase of the correlation length L_p according to an empirical fit. The proposed values are presented in Table 3.2.

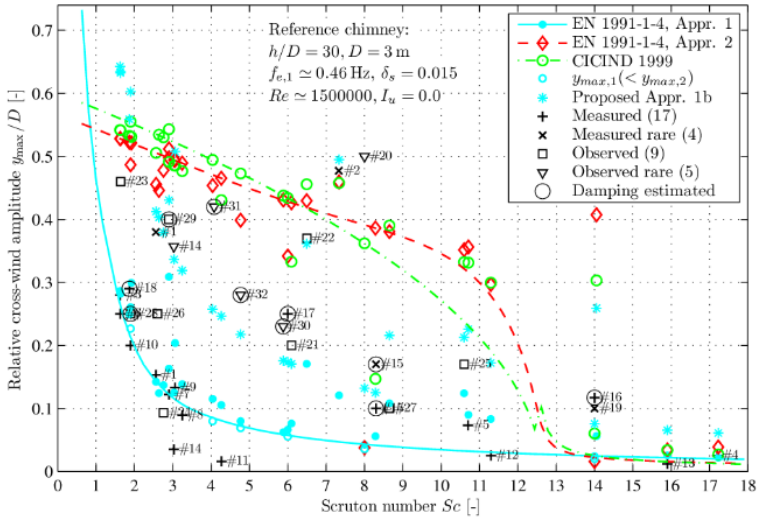


Figure 3.10: Comparison of predicted and measured/observed cross-wind amplitudes [13]

Table 3.2: Values of correlation length L_p for extreme events according to Clobes [13]

L/d	y_0/d
12	≤ 0.05
30	≥ 0.2

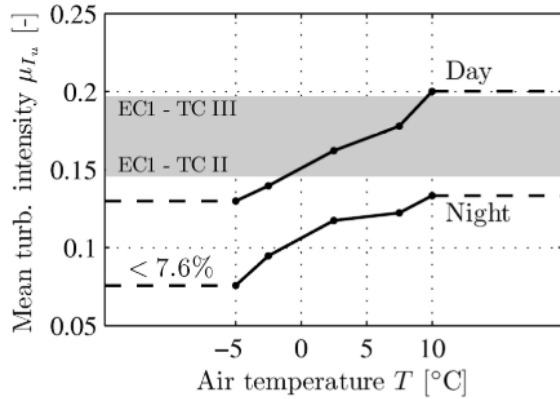


Figure 3.11: Influence of air temperature on turbulence intensity [13]

Finally, some researchers propose also the reduction of Strouhal number S_t from

0.18 to 0.16 for modelling extreme events. This leads to higher critical wind velocities V_{cr} , resulting directly to higher excitation forces. Concluding, this modification of the effective length is based on observed/measured amplitudes from industrial chimneys. Even if the modification of the parameter is mostly empirical, the results of this method will be presented for comparison reasons in Chapter 5.

Chapter 4

Spectral models

In this Chapter, the theoretical background behind the spectral models is presented. It is mainly based on Vickery & Basu [64] mathematical model, which is the base of the spectral models. They are called spectral models because the vortex shedding load has a spectral density centered around the vortex shedding frequency. The aeroelastic interaction in this approach is modelled through a damping modification. Presentation of experimental results published by Lupi [33] are following, including the derived analytical model. Afterwards, another approach resulted by processing the same experimental data through a different perspective is explained. Concluding this Chapter, a formulation for implementing the spectral models is presented, considering the tapered section of the wind turbine tower and different wind profiles at a range of wind velocities.

4.1 Vickery & Basu model

As mentioned from Vickery & Basu [64], tall slender structures with circular cross-section, such as towers, chimneys e.t.c., respond dynamically under wind loading in the across-wind direction. In spectral models, random vibration theory is applied. However, it is adequate only for small vibration amplitudes, while for higher ones it yields unconservative results. Therefore, a modification is required and is implemented through the reduction of the system's damping, modelling in the way the fluid structure interaction.

After years of research, in 1983 a new model for the prediction of the across-wind vibrations was presented by Vickery & Basu [65],[6]. It is a semi-empirical mathe-

mathematical model which was developed for structures with cylindrical cross-sections of variable diameter, which vibrate in a mode of arbitrary shape and are subjected to turbulent flow.

4.1.1 Theoretical background

In this section, the theory behind spectral models is based on Vickery, Basu and Clark's research. More recent researchers base their experiments and models on their observations and assumptions. Thus, the theoretical background of their model is presented here as the base case for this approach.

According to measurements in smooth flow, Vickery and Basu observed the existence of two separate fluctuating forces. The first one arises from the shedding of the vortices and is always present, even if the cylinder is not vibrating. These forces are described within the framework of linear-vibration theory as long as the amplitudes are small. The second one arises from the motion of the cylinder and these forces are called motion-induced forces. These are becoming significant at larger amplitudes of oscillation.

The most important feature of this model is the representation of the motion-induced forces by a nonlinear aerodynamic damping force which is superimposed upon a narrow-band random force which represents the vortex shedding force on a stationary cylinder.

Vortex shedding forces

The vortex shedding force is represented as a fluctuating lift force. According to measurements, this force, even in smooth and uniform flow, is not strictly periodic, but has a spectral density. The spectrum of that force is concentrated around the Strouhal frequency f_{st} (see equation 2.1) and its bandwidth depends on turbulence intensity as it is illustrated in Figure 4.1.

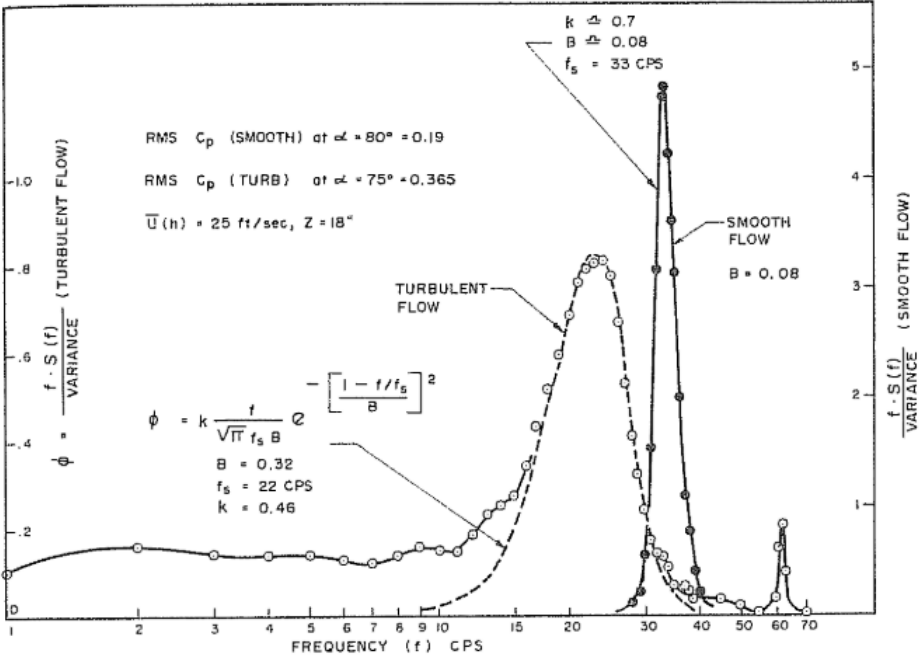


Figure 4.1: Spectrum of lift force fluctuations [67]

The turbulence is represented to have a Gaussian form and the lift force to be almost sinusoidal in smooth flow, as it still has a bandwidth. Therefore, the resulting force takes also a Gaussian form. Experimental results were fitted by Vickery and Clark [67] (see Figure 4.1) and equation 4.1 was derived which describes the spectrum of the lift force $S(f)$.

$$\frac{S(f)}{\tilde{C}_L^2} = \frac{1}{\sqrt{\pi} B f_s} e^{-\left[\frac{1 - \frac{f}{f_s}}{B}\right]^2} \tag{4.1}$$

where B is the bandwidth and a measure of the spread of the spectrum. This bandwidth based on experimental data can be computed by equation 4.2. \tilde{C}_L is the rms of the lift coefficient.

$$B^2 = B_0^2 + 2 \frac{\tilde{w}}{V} \tag{4.2}$$

$$\tilde{w} = \frac{1}{2} \rho V^2 D \tilde{C}_L \tag{4.3}$$

where $B_0 = 0.05 - 0.1$ is the bandwidth in the smooth flow and \tilde{v} is the rms of the wind velocity. Finally, the fluctuating lift force is expressed by equation 4.3.

Motion-induced forces

The motion of a structure has the effect of introducing some aeroelastic effects. The principal characteristics of the lock-in phenomenon, according to Vickery and Basu, are the increase of the magnitude of the fluctuating force and the increase of the correlation length with increasing amplitude. In this model, these features are incorporated by introducing a negative aerodynamic damping term.

The aerodynamic lift force, based on experiments from Scruton [52], is expressed as:

$$w(t) = h_a y + k_a \dot{y} \quad (4.4)$$

where h_a and k_a are the in-phase coefficients with the displacement and the velocity respectively. It should be mentioned that the equation 4.4 does not contain the vortex shedding forces (see equation 4.3) presented previously. Therefore, assuming harmonic motion ($y = Y \sin(2\pi f_0 t)$) and nondimensionalizing h_a and k_a equation 4.4 transforms to equation 4.5:

$$w(t) = \frac{1}{2} \rho V^2 DC_L + 8\pi^2 f_0^2 \rho D^2 \cdot [H_a \cdot Y \sin(2\pi f_0 t) + K_a \cdot Y \cos(2\pi f_0 t)] \quad (4.5)$$

The in-phase component H_a is called aerodynamic stiffness. Its value, even it is comparable to K_a , is negligible compared to the mechanical stiffness of the system. The out-of-phase component K_a is called aerodynamic damping and depends on the turbulence intensity and the amplitude of vibration. K_{a_0} is denoted as the value of K_a at small vibration amplitudes. The dependence of K_a on turbulence intensity and flow velocity is illustrated in Figure 4.5.

The effect of turbulence intensity and flow velocity on aerodynamic parameter K_a is taken into account according to Figure 4.5 and is implemented following the equation 4.6.

$$K_a(z) = K_{a_0, max}(z) (1 - 3I_v(z)) \left[2 \left(\frac{V_m(z)}{V_{cr}(z)} \right)^2 - 7 \frac{V_m(z)}{V_{cr}(z)} + 6 \right] \quad (4.6)$$

It was previously mentioned that one of the effects of the motion of the structure is the increase of the force correlation along its length. According to Figure 4.2, Vickery and Basu assumed no correlation between the motion induced and the

vortex shedding forces. In cases where $f_0/f_{st} \neq 1$, two distinct forces can be identified and this assumption can be justified. In case of $f_0/f_{st} \simeq 1$, a single peak is observed and the assumption is not valid anymore. Nevertheless, it is assumed that two forces coexist and at high amplitudes of vibration the motion induced forces engulf the vortex-shedding ones (see Figure 4.3). Vickery and Basu, justifying their assumption, mentioned that their intention is to produce a mathematical model that will reproduce the gross features of vortex-induced vibration and not the detailed physics.

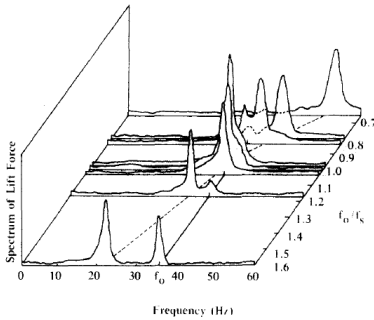


Figure 4.2: From of the lift force in the frequency domain for varying f_0/f_s

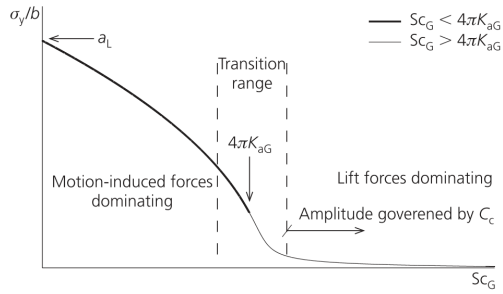


Figure 4.3: Interpretation of aerodynamic forces versus Scruton number [25]

Therefore, the assumption of no correlation between “stationary” vortex-shedding and motion induced forces allows to express the rms value of the lift force per unit length by equation 4.7.

$$\tilde{w}^2 = (1/2\rho V^2 D \tilde{C}_L)^2 + 2[(2\pi f_0)^2 \rho D^2 H_a Y]^2 + 2[(2\pi f_0)^2 \rho D^2 K_a Y]^2 \quad (4.7)$$

where \tilde{C}_l is the rms of the lift coefficient. Normalizing the above equation results to equation 4.8.

$$\frac{\tilde{w}^2}{(1/2\rho U^2 D)^2} = \tilde{C}_L^2 + A^2 \quad (4.8)$$

A represents the motion induced forces and \tilde{C}_L the vortex shedding forces. A simple criterion was adopted: when $A^2 < \tilde{C}_L^2$ the shedding frequency is given by the Strouhal relationship and when $A^2 > \tilde{C}_L^2$ by the vibration frequency.

Motion-induced forces at large amplitudes

According to experimental results of vibrating cylinders presented by Feng [20], the non-linearity of the motion induced forces (A), as a function of the amplitude, can be observed in the lock-in range (see Figure 4.4). Furthermore, even for values of structural damping close to zero, a self-limiting response of the system is observed. This confirms the belief of the self-limited nature of the phenomenon.

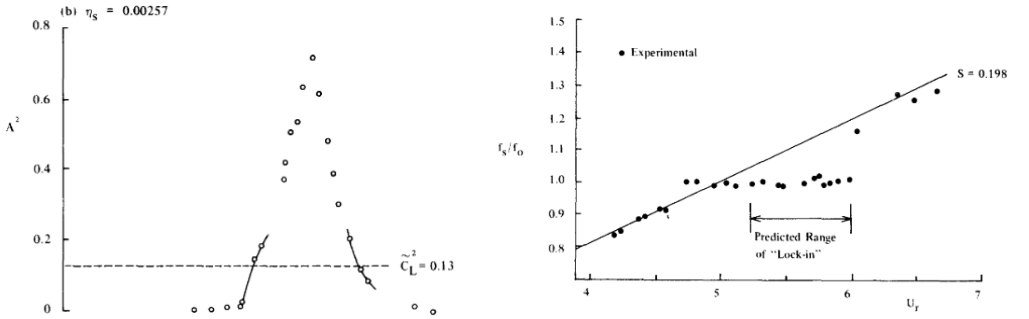


Figure 4.4: Nonlinear form of motion induced forces A and prediction of lock-in range in comparison with experimental results [20]

In order to formulate the non linear behavior of the motion induced forces, firstly, the negative aerodynamic damping is expressed as a fraction of the structural damping of the system. K_a is considered as the aerodynamic damping coefficient. According to Marris [34] the aerodynamic damping force is expressed by equation 4.9.

$$w(t) = k_a(\dot{y} - G\dot{y}^3) \Rightarrow w(t) = k_a\dot{y} \left[1 - (Y/Y_L)^2 \right] \quad (4.9)$$

where G is a constant. The nonlinear term ensures the self limiting amplitude of the vibration. Assuming an oscillation ($y(t) = Y(t)\cos(2\pi f_0 t)$), where $Y(t)$ is a slowly varying function of time, equation 4.9 transforms to its right hand side. Y_L is the limiting amplitude of the system without structural damping and external forcing. Finally, considering random excitation the damping force is simplified as follows:

$$F(t) = k_a\dot{y} \left[1 - \left(\frac{\tilde{y}}{\tilde{y}_L} \right)^2 \right] \Rightarrow \zeta_a = -\frac{\rho D^2}{m} K_{a0} \left[1 - \left(\frac{\tilde{y}}{\tilde{y}_L} \right)^2 \right] \quad (4.10)$$

where $\tilde{y}_L = Y_L/\sqrt{2}$. This means linear damping coefficient which depends on the mean-square of the displacement \tilde{y}^2 averaged over a long period. The negative

aerodynamic damping as a fraction of the critical is expressed by equation 4.10. The dependence of the negative aerodynamic parameter K_a on the vibration amplitude is illustrated in Figure 4.6.

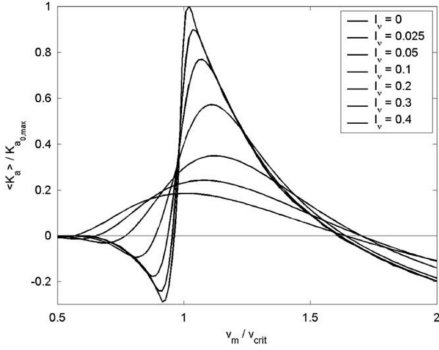


Figure 4.5: Influence of turbulence intensity I_v and ratio V_m/V_{cr} on K_{a0} [63]

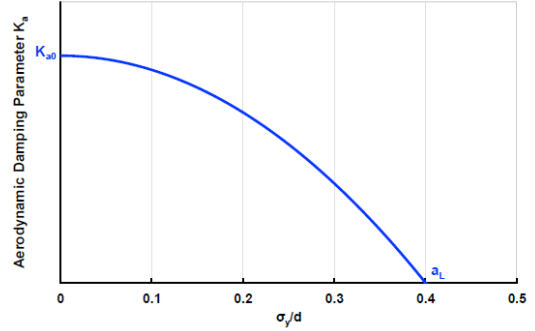


Figure 4.6: Aerodynamic parameter K_a according to Vickery & Basu [65]

K_{a0} is the linear part of the equation, depends on Re , turbulence intensity I_v and the ratio of mean wind speed and critical one ($K_{a0} = \Phi\left(\frac{\bar{u}}{f_0 d}, I_v, Re\right)$) and refers to small oscillation amplitudes. The final expression for the calculation of the vibration amplitude according to this model becomes:

$$\frac{y_{rms}}{D} = \frac{\tilde{C}'_L^2}{8\pi^2} \left(\frac{V}{f_n D}\right)^2 \frac{\rho D^2}{m} \left[\left(\frac{\sqrt{\pi} f_n}{4B f_s}\right) \frac{e^{-[(1-f_n/f_s)/D]^2}}{(\zeta_s + \zeta_a)} \right]^{0.5} \quad (4.11)$$

where \tilde{C}'_L^2 is the sectional rms lift coefficient.

4.2 Damping-Modified Spectral method

In this section, a modified spectral model is presented as published by Lupi [33]. It is directly related to the work of Vickery and Basu, presented in the previous section. A set of forced-vibration experiments were performed in order to identify the aerodynamic damping as a function of the oscillation amplitude (see subsection 4.2.1). Afterwards, free oscillation experiments of a cantilever beam found to validate the measured aerodynamic forces (see subsection 4.2.1).

4.2.1 Wind tunnel tests

Forced oscillation experiments

The wind tunnel tests (see Figure 4.7) examined the fluid-structure interaction on a smooth and on a rough cylinder ($k/d = 0.013$), resulting to laminar (subcritical Re) and turbulent separation (transcritical Re) of the flow respectively. The flow velocity is kept constant at 3 m/s , varying the oscillation frequency to cover the “lock-in” range, following equation 4.12. In addition, the experiments were performed for various vibration amplitudes to derive the dependency of the aerodynamic parameter K_a on oscillating amplitude. It should be noted that this set of experiments is one of the few, if not the only one, with these cylinder’s dimensions ($L = 178 \text{ cm}$, $d = 0.15 \text{ m}$). According to literature (see section 2.2), the most commonly used diameter is $d = 50.8 \text{ mm}$, resulting to low measured amplitudes.

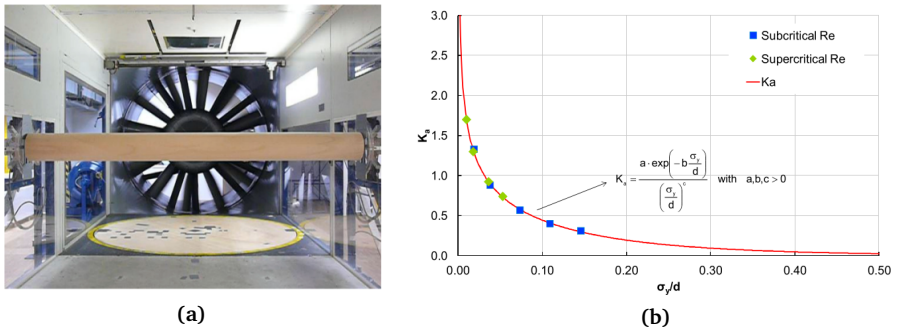


Figure 4.7: (a) Wind tunnel model in forced vibration experiments and (b) aerodynamic parameter K_a versus flow velocity [32]

In order to identify the aeroelastic forces, the forced vibration experiments were performed twice: firstly the cylinder is vibrating without the presence of the flow and secondly under wind. The measured forces contain an in-phase and an out-of-phase component. The difference between the two tests of the in-phase component, contains information about the aerodynamic stiffness h_a . In air, its contribution is insignificant and negligible for design purposes and therefore can be neglected [51]. The force component c_a , which is in phase with the velocity, referred also as the quadrature component (separated in phase by 90°), is related to the damping of the system. In tests without flow, it contains contribution from structural and still air damping, while in presence of flow it corresponds to the total damping (struc-

tural+aerodynamic) of the system.

The forced oscillation experiment is described by the equation of motion of an oscillator with excitation force acting on its supports [14]. The equations of motion for the two type of tests are presented in equations 4.13 and 4.14. The flow velocity is kept constant in these experiments. The range of V/V_{cr} is covered by changing the vibration frequency of the mounted cylinder (see equation 4.12).

$$\frac{V}{V_{cr}} = \frac{V \cdot S_t}{f_1 \cdot d} \quad (4.12) \quad M\ddot{y} + c(\dot{y} - \dot{y}_s) + k(y - y_s) = 0 \quad (4.13)$$

$$M\ddot{y} + c_{eff}\dot{y} + k(y - y_s) = F_a(t) = c_a y + h_a y \quad (4.14)$$

where y is the motion of the mass, y_s is the motion of the support and F_a is the aeroelastic force. As presented by Lupi [32], after deriving the values of the aerodynamic damping coefficient c_a (kg/s) for every oscillation amplitude, the non-dimensional parameter K_a can be computed by equation 4.15.

$$\zeta_a = \frac{c_a}{2M\omega_n} \Rightarrow K_a = -\zeta_a \frac{m_{eq}}{\rho d^2}, \text{ where } K_a = 0.3475 \cdot \frac{\exp(-5.808 \cdot \frac{\sigma_y}{d})}{(\frac{\sigma_y}{d})^{0.3582}} \quad (4.15)$$

where M is the oscillating mass (kg) and m_{eq} is the equivalent mass per unit length (kg/m). The variation of K_a versus the vibration amplitude at critical flow velocity ($V = V_{cr}$) is presented in Figure 4.7b and in the fitted equation 4.15. The positive curvature of the K_a -curve can be observed, in contrast with Vickery's curve in Figure 4.6. In addition, absence of a limiting amplitude $a_L = 0.4$ is observed in those results.

Finally, the equation proposed [31] in order to compute the vibration amplitudes is presented as follows:

$$\frac{y_{max}}{d} = k_p \cdot \frac{\sigma_y}{d} = k_p \cdot \frac{1}{S_t^2} \cdot \left(\frac{V}{V_{cr}} \right)^2 \cdot \frac{\sqrt{C}}{\sqrt{\frac{Sc}{4\pi} - K_a}} \quad (4.16)$$

where C is the load parameter, expressed by equation 4.17. Based on experimental observations from free oscillation experiments (see section 4.2.1), the velocity V where maximum amplitude is observed depends on the Scruton number ($\frac{V}{V_{cr}} = 1.25$ when $Sc \leq 10$ and $\frac{V}{V_{cr}} = 1.00$ when $Sc > 10$). An explanation of this rule is presented in section 4.2.2.

$$C = 1.42 \cdot 10^{-4} \cdot \frac{d^3 \rho}{M_n} \cdot \lambda \cdot \frac{\sigma_{cL}^2}{B} \quad (4.17)$$

In addition, σ_y is the standard deviation of the displacement and after multiplication with a peak factor the vibration amplitude is obtained.

Free oscillation experiments

Afterwards, free oscillation experiments were performed on a cantilever beam in order to validate the obtained values of aerodynamic parameter K_a . The beam had a circular cross-section ($d = 50 \text{ mm}$, $h/d = 15.5$) and was subjected to a range of flow velocities in order to obtain the maximum displacement. The “lock-in” range is found between $0.9 \div 1.5 V_{cr}$. A peak factor of $k_p = 1.63$ (see Figure 4.8) is found which is justified due to the harmonic nature of the vibration.

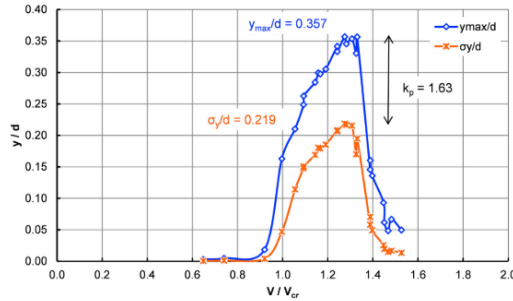


Figure 4.8: Free oscillation experiment in a cantilever beam [33]

According to Lupi [33], the standard deviation of the amplitude $\sigma_y = 0.219 \cdot d$ is predicted from the DMSM model ($\sigma_y = 0.221 \cdot d$), while the V&B model resulted to a much higher one ($\sigma_y = 0.382 \cdot d$). This difference on the computed amplitudes can be explained from the positive instead of negative curvature of K_a versus the oscillation amplitude. Comparing the Figures 4.7b and 4.6, one can realize that Vickery and Basu model “requires” higher amplitudes to reduce the motion induced forces modeled through the aerodynamic parameter K_a .

More detailed presentation of the experimental set-up, about the derivation of the aerodynamic parameter K_a and comparison with observed and measured vibration amplitudes of industrial chimneys can be found in the following [33], [31], [32].

4.2.2 Aerodynamic parameter K_a

In the previous section 4.2.1, the experimental results were briefly presented and discussed. In this section, the values of aerodynamic parameter K_a derived from that set of experiments will be presented, commented and also processed from a different perspective. The ultimate goal is to create a model adapted to the case of wind turbine towers with varying diameter along the height, as mentioned in the Introduction of this thesis. It should be noted that the computed values of K_a versus the flow velocity were shared by Lupi directly, for further analysis of the data. In the following Figure 4.9, measured and approximated values of the aerodynamic parameter are presented.

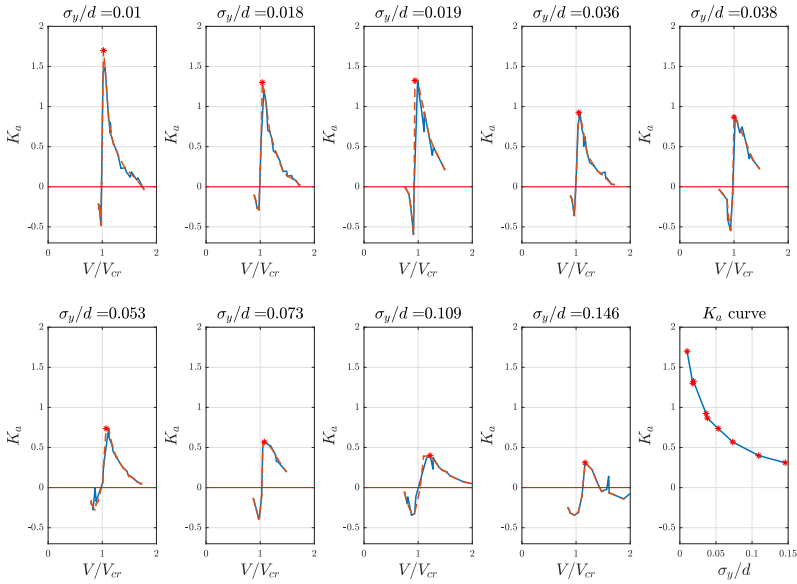


Figure 4.9: Measured (-) and approximated (-) aerodynamic parameter K_a for varying $\frac{V}{V_{cr}}$. Positive values represent a negative aerodynamic damping

In Figure 4.9, one can observe the increase of “lock-in” range with increasing amplitude. Moreover, the shift of $\frac{V}{V_{cr}}$ ratio to higher values than unity can be noticed at higher vibration amplitudes. Therefore, lower Sc number (lower damping),

meaning higher oscillation amplitudes, results to wider synchronization range and the maximum amplitude is found at higher velocities than the critical one. This explains the ratio $\frac{V}{V_{cr}} = 1.25$ for $Sc \leq 10$ which was proposed in equation 4.16. It should be noted that this proposal was made by experimental observations by the free oscillation tests (see subsection 4.2.1).

Another valuable information that can be extracted by these figures is the variation K_a with the flow velocity. This feature is not described by equation 4.15 and Figure 4.7b. In the case of wind turbine towers and tall chimneys as well, the wind velocity is not constant along their height. This comes in contrast to free oscillation experiments of cantilever models where the flow velocity is constant and shear flow is not applied. In addition, tapered section of the wind turbine tower amplifies the difference of the ratio V_m/V_{cr} over the height. Therefore, aiming to obtain more accurate predictions of the vibration amplitude of wind turbine towers subjected to VIV, the importance of including the variation of K_a with flow velocity is indisputable.

Subsequently to the aforementioned comments, the most suitable way to extract all the information from forced oscillation experiments is by firstly presenting the curves in a three-dimensional way, as in Figure 4.10. Afterwards, the curves were fitted and extrapolated to include higher vibration amplitudes, following the fitted equation 4.15. An interpolation curve was fitted to the experimental values in order to evaluate K_a for all the possible combinations of σ_y and reduced velocity V_r .

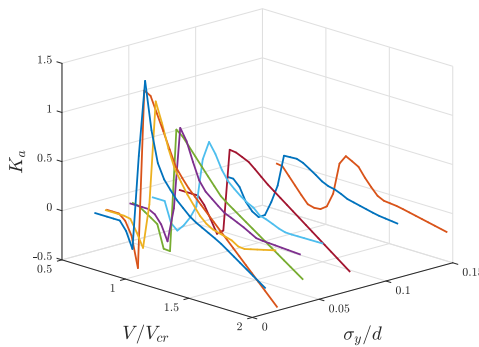


Figure 4.10: Aerodynamic parameter K_a for varying $\frac{V}{V_{cr}}$ and $\frac{\sigma_y}{d}$

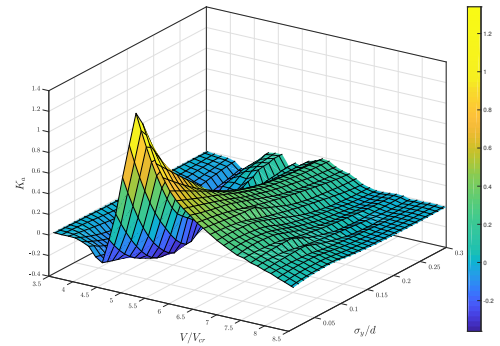


Figure 4.11: Fitted curve of aerodynamic parameter K_a

From the three-dimensional plot of the fitted surface, a contour plot can be eas-

ily obtained and presented in Figure 4.12. The resulted figure can be used as a “look-up” table for the calculation of Vortex Induced Vibrations. Assuming an amplitude, shape of vibration (e.g. first mode shape) and a wind profile, one can easily obtain the values of aerodynamic parameter K_a along the height of the structure. Therefore, the magnitude of motion-induced forces is illustrated for all the possible combinations of flow velocity and amplitude of vibration.

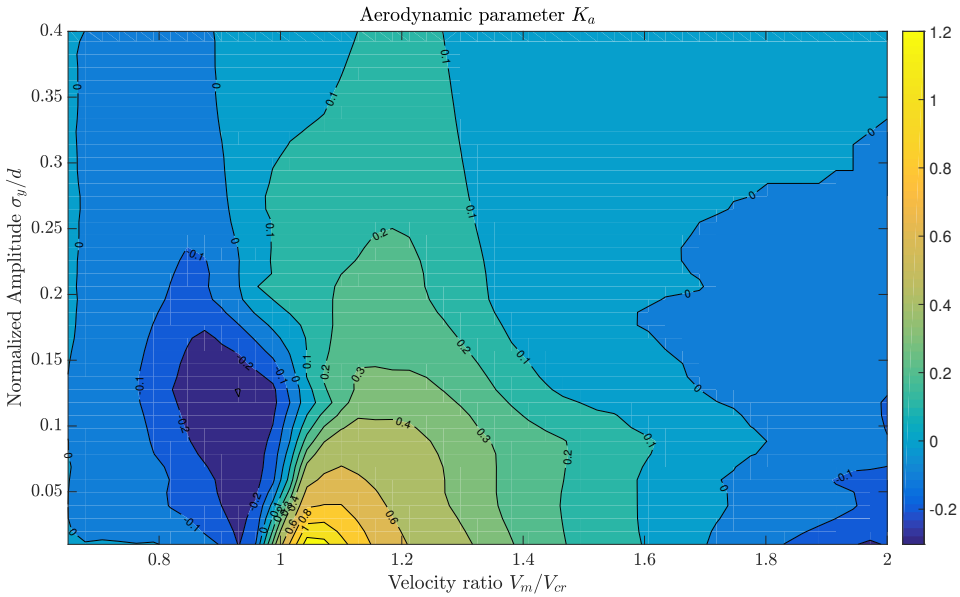


Figure 4.12: Contour plot of aerodynamic parameter K_a versus ratio of V/V_{cr} and oscillation amplitude. Positive values refer to negative aerodynamic damping.

The “blue” areas of the figure represent aeroelastic dissipation of energy, meaning increase of total damping of the system while the rest, the negative aerodynamic damping which opposes the structural one. Qualitatively, the contour plot can be verified with the free oscillation experiments (see Figure 2.10), presented in section 2.2.3. Moreover, Figure 4.12 can be compared with the contour plot presented by Hover [27] (see Figure 2.13) which was obtained from forced oscillation tests performed in a water channel. It can be observed from the contour plot that as the structural damping decreases (relevant to decrease of $K_a \downarrow$ in Figure 4.12):

1. The lock-in range increases

2. The vibration amplitude increases
3. Higher vibration amplitudes are found at higher flow velocities $V_r > 1$, phenomenon observed also in the free oscillation experiment (see Figure 4.8)

Concluding, this contour plot can justify the perspective of some researchers, that from forced oscillation tests, force coefficients can be extracted that can simulate the free oscillation ones. Their biggest contribution/difference is the value of force coefficient at areas which are not included in the free tests. These are roughly for values of reduced velocity $V_r < 1$ and $V_r > 1.7$. The importance of these values will become obvious in the next Chapter 5, where sections of the tower are found in those “areas”.

4.3 Model formulation

In this section, a model formulation from Verboom and van Koten [63] is presented. The following model was published considering the V&B model. However, it can be applied to other spectral models, since they refer to the same parameter aerodynamic parameter K_a . For reasons of clarification, the aerodynamic damping of a structure can be expressed in a form similar to the Scruton number by equation 4.18.

$$S_a = \frac{2\delta_a m_e}{\rho d^2}, \quad S_c = \frac{2\delta_s m_e}{\rho d^2} \quad (4.18)$$

where $K_a = \frac{-S_a}{4\pi}$. The aerodynamic damping can be higher than the structural, but since the solution is found in the frequency domain (steady state solution), its maximum value is the structural damping. In the following Figure 4.13, the effect of different values of δ_a on vibration, in absence of lift force, is illustrated.

The response of the system can be calculated by superimposing the responses of all modes. Regarding the wind turbine towers, the response can be computed considering only the first mode of vibration, since the second natural frequency corresponds to extremely high wind velocities. Furthermore, the frequency content of the lift force is following the Strouhal relationship, resulting to frequencies far from the fundamental one. Therefore, for a system with one DOF the squared standard deviation of the deflection is given by Basu (1982) [7] (see equation 4.19).

$$\sigma_y^2 = \int_0^\infty |H(\omega)|^2 \cdot S_{wv}(\omega) d(\omega) \approx S_{wv}(\omega_0) \frac{1}{4KC} = \frac{1}{8 \omega_0^2 \zeta M^2} S_{wv}(\omega_0) \quad (4.19)$$

$$|H(\omega)|^2 = \frac{1}{K^2} \frac{1}{1 - \left(\frac{\omega_s}{\omega_n}\right)^4 + 4\zeta^2 \left(\frac{\omega_s}{\omega_n}\right)^2} \quad (4.20)$$

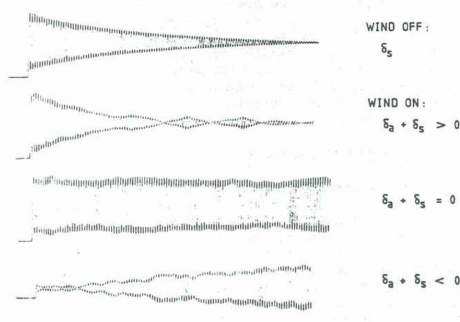


Figure 4.13: Typical damping curves obtained at different velocity ratios [12]

where $H(\omega)$ is the frequency response function of the system, S_{wv} is the spectrum of the generalized lift force, ω_n is the natural angular frequency of the tower. K and C are the modal stiffness and modal damping, ζ is the generalized damping normalized with the critical damping and M is the modal mass of the tower. Dyrbye and Hansen (1997) [17] presented an approximation of $S_{wv}(\omega_0)$:

$$S_{wv}(\omega_0) \approx 2 \lambda D_r \int_0^h g^2(\omega_n, z) dz \quad (4.21)$$

λD_r denotes the load correlation length, where λ is often found to be near unity or a little greater. $g(\omega_n, z)$ is the spectrum of the fluctuating lift force at the resonance frequency. Presence of large scale turbulence produces broadening of the spectral peak, as stated by Vickery and Clark [67]. The form of the spectral peak is described by equation 4.22, as explained in subsection 4.1.1.

$$g(f, z) = \frac{\frac{1}{2} \rho V_m^2 D(z) C_L(z) \cdot \Phi(z)}{\sqrt{\sqrt{\pi} B(z) f_s(z)}} \exp \left[-\frac{1}{2} \left(\frac{1 - f/f_s(z)}{B(z)} \right)^2 \right] \quad (4.22)$$

where $B(z)$ is the width of the lift spectrum, $D(z)$ the diameter, $V_m(z)$ the mean wind velocity and C_L is the r.m.s. of the lift coefficient. C_L depends on the Re and is obtained from Table 4.1. The width of the lift spectrum is computed as $B = 0.1 + I_v(z) \leq 0.35$, depending only on the turbulence intensity I_v .

The total damping of the system is the summation of the structural and the aerodynamic damping. The generalized aerodynamic damping normalized by the critical damping is expressed in the following extended formulation [7]:

Table 4.1: RMS lift coefficient C_L as a function of the Re number

$Re \leq 2 \times 10^5$	$Re = 2 \times 10^5$	$Re \geq 1 \times 10^6$
C_L	0.7	0.2

$$\zeta_a = \rho \int_0^h \frac{D^2(z) K_a(z) \Phi^2(z)}{M} dz = \frac{\rho \cdot D_r^2 \cdot K_{a,r} \cdot c_3}{m_e} \quad (4.23)$$

where $K_{a,r}$ is the value of K_a at the reference point (maximum deflection), m_e is the equivalent mass per unit length (kg/m). The coefficient c_3 (see equation 4.24) takes into account the values of aerodynamic parameter K_a and diameter D along the height of the structure, assuming that the structure is vibrating in the first mode shape.

$$c_3 = \frac{\int_0^h K_a(z) D^2(z) \Phi^2(z) dz}{K_{a,r} D_r^2 \int_0^h \Phi^2(z) dz} \quad (4.24) \quad m_e = \frac{\int_0^h m(z) \Phi^2(z) dz}{\int_0^h \Phi^2(z) dz} \quad (4.25)$$

The values of K_a along the height of the structure are obtained either by Figure 4.6 or by 4.7, depending on the applied model, Vickery and Basu or Lupi's one. Afterwards, due to turbulence intensity and the ratio of mean over the critical wind velocity these values are reduced for every cross-section along the height (see Figure 4.5 and equation 4.6). Alternatively, the contour model of the K_a values can be applied directly (see Figure 4.12). In this case, except for the negative aerodynamic damping, positive one results in cases when $\frac{V}{V_{cr}} \leq 1$ or ≈ 1.7 . Furthermore, it should be noted that the DMSM is formulated by considering the maximum values of K_a obtained at different V_m/V_{cr} ratios. Therefore, the contour model represents the experimental results more accurately. Afterwards, the effect of turbulence intensity I_v can be applied.

The final equation obtained by substituting equations 4.21 - 4.25 into equation 4.19 is formulated:

$$\begin{aligned} \sigma_y^2 &= \frac{\lambda D_r \int_0^h g^2(f_0, z) dz}{4 \cdot \omega_0^3 \cdot M^2 (\zeta_s - \zeta_a)} = \frac{\lambda D_r \int_0^h g^2(f_0, z) dz}{4 \cdot \omega_0^3 \cdot M^2 \left(\zeta_s - \frac{\rho \cdot D_r^2 \cdot K_{a,r}}{m_e} c_3 \right)} \\ &= \frac{C_a}{\frac{S_c}{4\pi} - \frac{\int_0^h K_a(z) D^2(z) \Phi^2(z) dz}{D_r^2 \int_0^h \Phi^2(z) dz}} \end{aligned} \quad (4.26)$$

where C_a contains the information for the lift force and expressed by equation 4.27.

$$C_a = \frac{\lambda \int_0^h g^2(f_0, z) dz}{4 \cdot \omega_0^3 \cdot \rho \cdot D_r \cdot m_e \left(\int_0^h \Phi^2(z) dz \right)^2} \quad (4.27)$$

The maximum deflection at the tower top is derived by multiplying the standard deviation of the displacement with a peak factor k_p (see equation 4.28), which depends on the type of vibration. For a structure with stochastic response, its value is equal to four and for a harmonic response with constant amplitude equal with $\sqrt{2}$. The aerodynamic parameter $K_{a,0}$ refers to zero vibration amplitude [46].

$$y_{max} = k_p \cdot \sigma_y = \sqrt{2} \cdot \left[1 + 1.2 \arctan \left(0.75 \left(\frac{Sc}{4\pi K_{a,0}} \right)^4 \right) \right] \cdot \sigma_y \quad (4.28)$$

The values of the peak factor versus the ratio $\frac{Sc}{4\pi K_{a,0}}$ are presented in Figure 4.14.

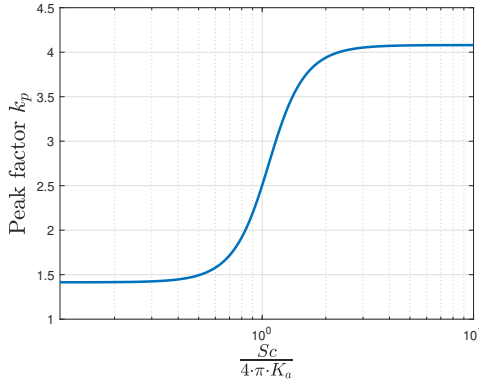


Figure 4.14: Peak factor k_p

Concluding, it should be noted that for the three models, the vibration amplitude is computed through an iterative procedure, as the aerodynamic parameter K_a depends on the standard deviation of the displacement. A flow chart (see Figure A.1) for the implementation of the spectral approaches is presented in Appendix A explaining this iterative procedure. In Chapter 5 this formulation becomes more clear as the intermediate steps are presented in detail.

Chapter 5

Study case of Vortex Induced Vibrations on wind turbine towers

5.1 Study case

In the Introduction (Chapter 1), it was mentioned that the scope of this thesis is the accurate prediction of Vortex Induced Vibrations on wind turbine towers. There are a number of load cases to which the offshore wind turbines are subjected as mentioned previously, before being commissioned in the offshore wind farm. These cases can be modeled by implementing different foundation stiffness, resulting to different natural frequencies. In this chapter, the case of towers on the quay side will be examined, as the other two cases have the beneficial effect of shorter time frame, wave and vessel's motion disturbance. The results presented in this Chapter are non-dimensional for confidential reasons. Comparison of the various models will be presented and sensitivity analysis of those will be performed considering the most influencing input parameters.

5.1.1 Structural modeling

The tower is modeled using finite elements according to Timoshenko beam theory. In Figures 5.1 and 5.2, the tower diameter along the height and the first two mode

are presented.

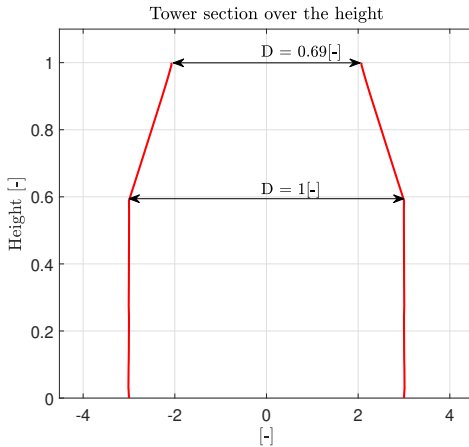


Figure 5.1: Tower diameter along the height

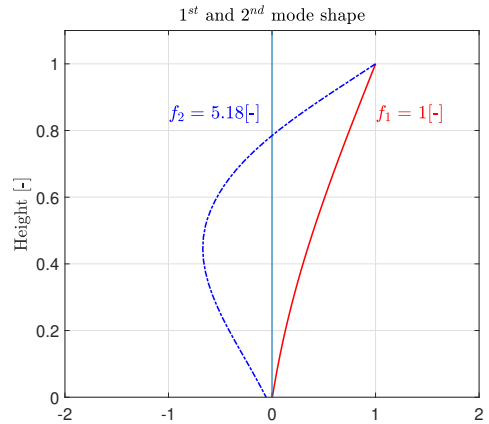


Figure 5.2: First and second mode shape of the tower

The towers are supported by different means depending on the situation. At the harbor the towers are mounted on the so-called “elephant feet” which is a frame where the towers are bolted to. This support is modeled through rotational and translational springs. The selected foundation stiffness, regarding the harbor case, is found in equation 5.1.



Figure 5.3:
Illustration of tower support

$$K_{rot} = 400 \text{ MNm/degree} \quad (5.1)$$

As for the structural damping (logarithmic decrement) of the steel towers in the fundamental mode according to Eurocode [4], a value of $\delta_s = 1.2 \%$ is proposed.

In the following sections, an analysis of vortex-induced vibrations will be presented for the aforementioned tower considering base values for the main input parameters. Afterwards, a parametric analysis will be performed. The values of the main parameters are summarized in Table 5.1.

Table 5.1: Input parameters for spectral models

Input parameters	value
Structural damping (log dec)	1.2 [%]
Strouhal number	0.18 [-]
Wind shear exponent	1/7 [-]
Turbulence intensity (mean)	8.5 [%]
Natural frequency (f_n)	1.00 [Hz]
Air density ρ_{air}	1.235 [kg/m ³]

5.1.2 Wind characteristics

In the previous chapter, according to the formulation of the spectral models, the importance of the wind characteristics is noted. The accurate implementation of spectral models requires not a single value for the wind velocity but a wind profile which will represent a realistic case. Furthermore, wind turbulence is a major input parameter affecting significantly the vibration amplitude of the towers. The wind shear exponent a is selected for the description of the wind profile in order to be directly related with its “steepness”. In Table 5.2, the values of the shear exponent according to the surrounding terrain are presented.

Table 5.2: Wind shear exponent [3]

Terrain	Wind Shear Exponent
	a
Open water	0.1
Smooth, level, grass-covered	0.15
Row crops/Low bushes with a few trees	0.2
Several buildings/Hilly, mountainous terrain	0.25

Turbulence intensity $I_v(z)$ along the height depends on the roughness length of the terrain z_0 . It is calculated through equation 5.2 and it should be noted that except for the reduction of the aerodynamic parameter K_a , it broadens the spectrum of the lift force B .

$$I_v = \frac{1}{c_0} \frac{k_l}{\ln(z/z_0)} \quad (5.2)$$

52 5. STUDY CASE OF VORTEX INDUCED VIBRATIONS ON WIND TURBINE TOWERS

where c_0 is the orography coefficient and k_l the turbulence intensity factor. The values of turbulence intensity I_v and shear exponent a should be selected appropriately in the design phase of the towers, as the vibration amplitudes are strongly dependent on these parameters. For the base case presented here, the resulting wind profile along with the critical velocity and turbulence intensity over the height are presented in Figures 5.4 and 5.5.

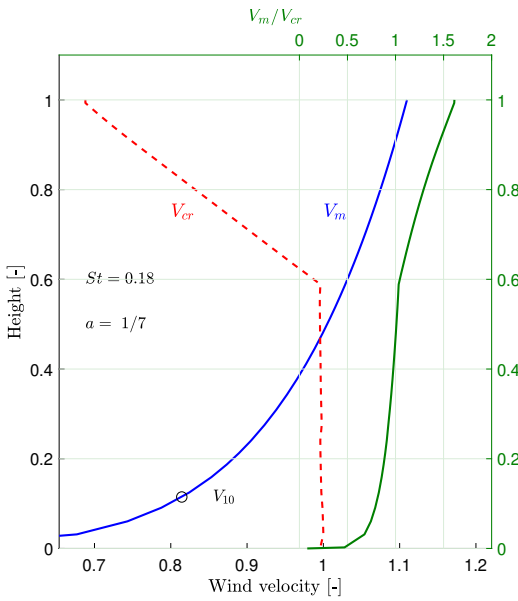


Figure 5.4: Wind profile (-), critical velocity (-) and the resulting V_m/V_{cr} ratio (-)

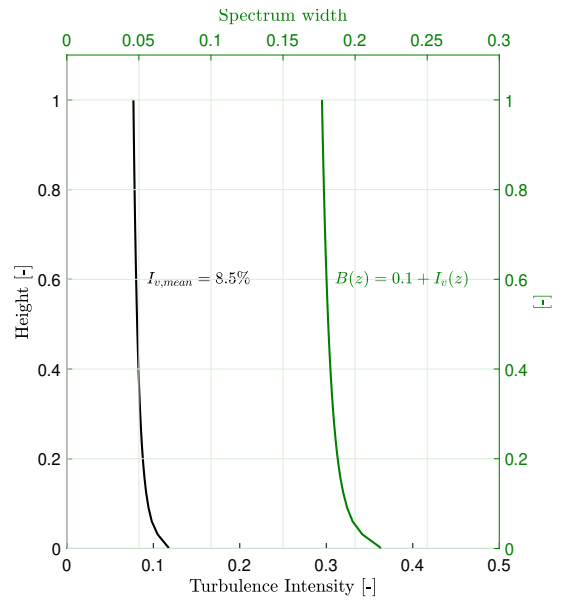


Figure 5.5: Turbulence intensity (-) and resulting width of lift spectrum (-)

It should be mentioned that in order to derive the maximum deflection of the tower due to VIV, an iteration over a range of wind velocities is performed. In Figures 5.4 and 5.5, the “critical” wind profile is presented, meaning the wind velocity (V_{10} at 10 m height) from which the maximum vibration amplitude was derived. In the next Figures 5.6 and 5.7, the lift force and the modal lift force are presented as computed by equations 4.22 (squared value $g(\omega_n, z)^2$) and 4.21 respectively.

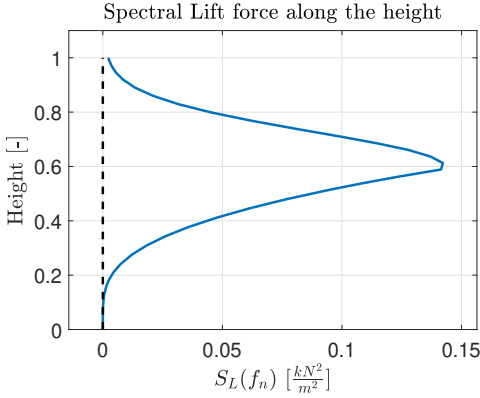


Figure 5.6: Spectral lift force along the height of the tower

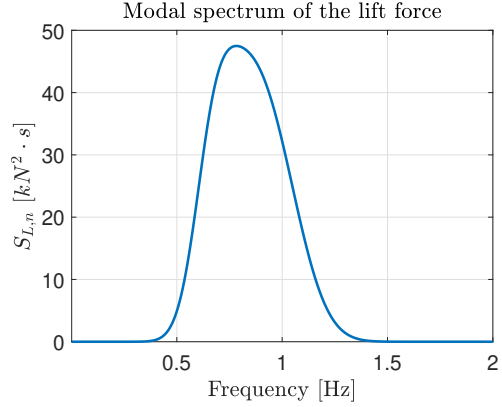


Figure 5.7: Modal lift force computed for the “critical” wind profile

5.1.3 Aerodynamic damping ζ_a

The fluid structure interaction, in spectral models, is modeled through negative aerodynamic damping ζ_a . As mentioned in the previous section, from an iterative procedure over a range of wind velocities, according to each model (V&B, DMSM or contour model) the maximum amplitude is computed. In order to compute the aerodynamic parameter K_a , a range of vibration amplitude is assumed for the tower, as by equation 4.26 the vibration amplitude cannot be directly computed. The tower is vibrating in the first mode shape as the lift force spectrum follows the Strouhal relationship and the second natural frequency is approximately five times higher than the first one. Consequently, the deflection of each section along the height of the tower can be defined. The solution is found when the assumed standard deviation is equal to the computed one ($\sigma_{y,assumed} \simeq \sigma_{y,computed}$).

The aerodynamic parameter $K_a(z)$ is computed according to the assumed vibration amplitude and the Figures 4.6 (V&B), 4.7b (DMSM) and 4.12 (contour model). As described in section 4.3, the values of K_a for the first two models are reduced according to $V_m(z)/V_{cr}(z)$ ratio and turbulence intensity $I_v(z)$ following the equation 4.6. The approach considering the contour plot requires only the reduction due to I_v as it includes the dependence on velocity ratio. In Figure 5.8, $K_a(z)$ is presented as computed for the three approaches. It can be observed that the “critical” wind profile (max computed amplitude) is different from the three methods and K_a extends at different part of the structure.

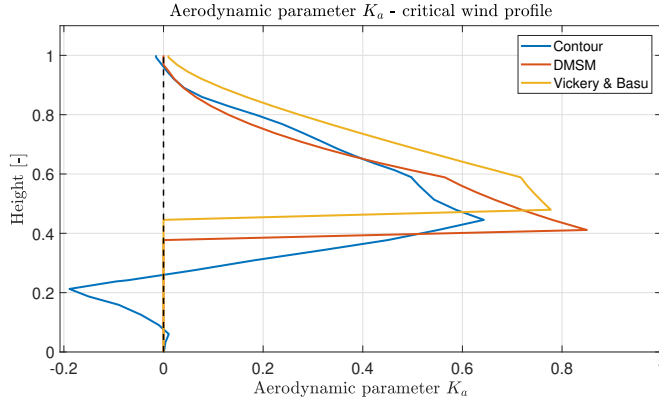


Figure 5.8: Aerodynamic parameter $K_a(z)$ according to V&B and DMSM

The most significant difference of using the contour plot, is the positive effect of aerodynamic damping at some extend of the structure. This derives from combinations of amplitude and velocity ratios which “fall” into the negative values in Figure 5.9. In this case, below 30 % of the tower height, the wind profile velocity is lower than the critical one ($V_m < V_{cr}$), resulting to increase of structural damping. It should be noted that the contour model is closer to the real nature of the VIV phenomenon and in this thesis it is considered the selected realistic and trustworthy approach.

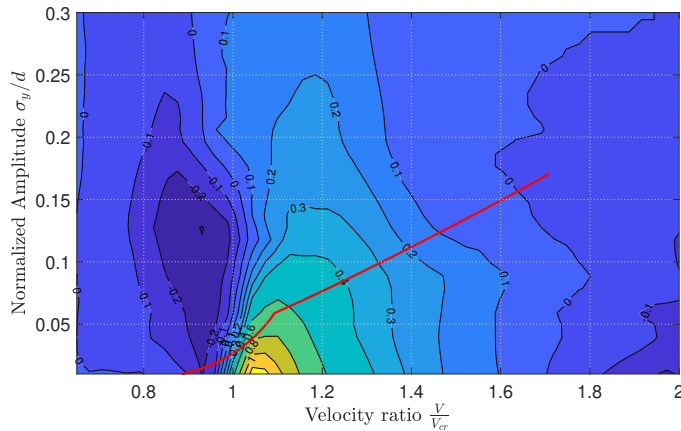


Figure 5.9: Aerodynamic parameter $K_a(z)$ according to contour model

Afterwards, the aerodynamic damping ζ_a is computed by equation 4.23. The total damping of the system is $\zeta_{total} = \zeta_s - \zeta_a$ and is always positive. For towers with low structural damping and low mass, the solution is found at almost zero total damping. For this tower where $\zeta_s = 1.2 \%$ the solution found for $\zeta_{total} = 0$, according to the three spectral models and is shown in Figures 5.10, 5.11 and 5.12.

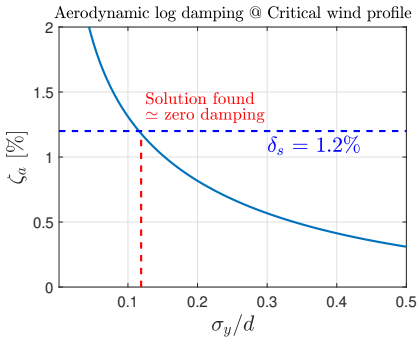


Figure 5.10: Negative aerodynamic damping ζ_a according to DMSM

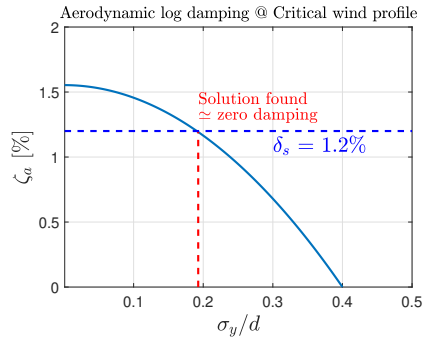


Figure 5.11: Negative aerodynamic damping ζ_a according to V&B model

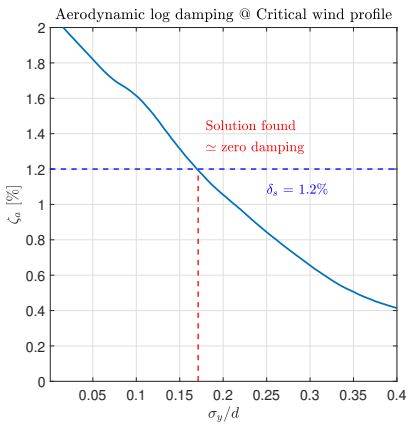


Figure 5.12: Negative aerodynamic damping ζ_a according to contour model

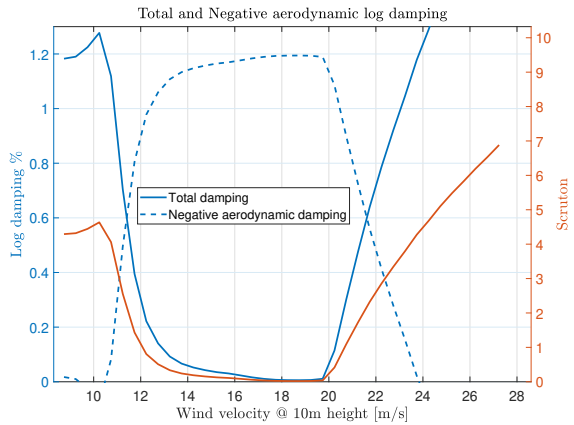


Figure 5.13: Total damping versus wind velocity at 10m height (contour model)

From the figures above, one can notice that the solution found by V&B model ($\sigma_y/d = 0.18$) is more conservative than DMSM ($\sigma_y/d = 0.119$), while for the contour model is found in the middle ($\sigma_y/d = 0.171$). In Figures 5.14, 5.15 and 5.13, the evolution of the total damping of the system over the wind velocity at 10 m height is plotted for the three models.

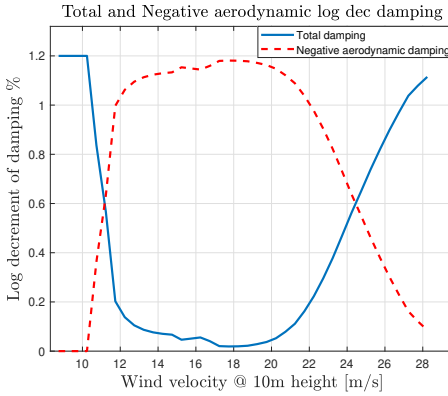


Figure 5.14: Total damping versus wind velocity at 10m height (DMSM)

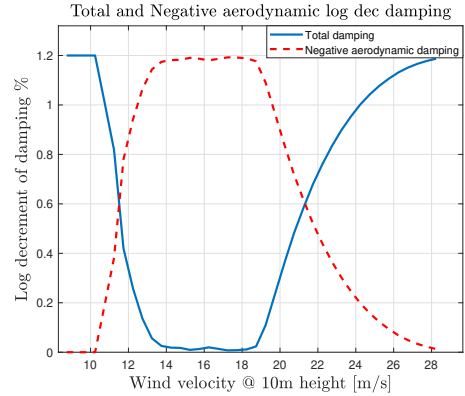


Figure 5.15: Total damping versus wind velocity at 10m height (V&B)

It can be observed (see Figures 5.14 and 5.15) that the aerodynamic damping is slightly higher for the V&B model for the critical range of velocities. However, at higher wind velocities, in this case over 21 m/s , its value is lower than DMSM. This can be explained from the comparison of the aerodynamic damping ζ_a (see Figures 5.10 and 5.11). At this range of velocities the vibration amplitude is low. The values of K_a according to DMSM goes to infinity in contrast to V&B and contour models where they are limited to a certain value.

Moreover, one can observe the increase of the damping to values higher than the structural one ($\delta_{tot} > \delta_s = 1.2\% \text{ logdec}$) at certain range of wind velocities (see Figure 5.13) in the case of the contour model. This is derived from the negative values of the contour plot leading to positive damping. Thus, the self-limiting nature of the VIV phenomenon is proved.

For the calculation of the vibration amplitude, at each step of the wind velocity the frequency response function (FRF) is computed. The standard deviation of the displacement is derived by equation 4.19 by multiplying the spectrum of the modal lift force (see Figure 5.7) with the frequency response function. The FRF for the

critical wind velocity is plotted in the next Figures 5.16 and 5.17.

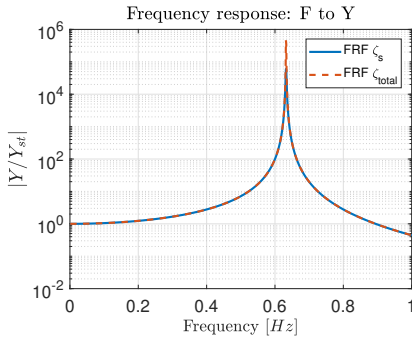


Figure 5.16: Frequency response function of the system

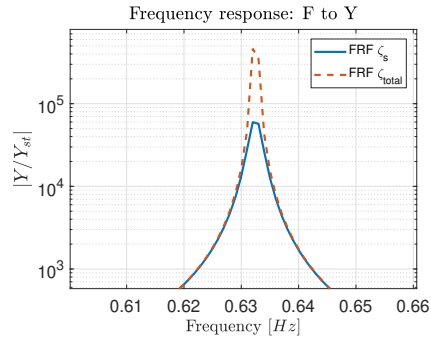


Figure 5.17: Effect of ζ_a at resonance frequency

Finally, the standard deviation and the displacement at tower top are presented in Figures 5.18, 5.19 and 5.20 as derived from the models for the selected range of wind velocities. The evolution of the peak factor versus the wind velocity is also illustrated. One can notice that at lower and higher wind velocities than the peak amplitude the value of the peak factor is closer to four due to the stochastic response of the system.

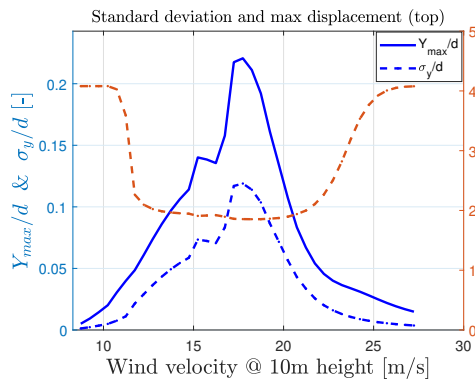


Figure 5.18: Standard deviation, peak factor and maximum displacement at the tower top (DMSM)

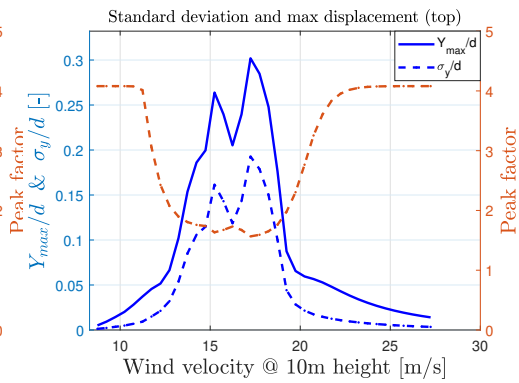


Figure 5.19: Standard deviation, peak factor and maximum displacement at the tower top (V&B model)

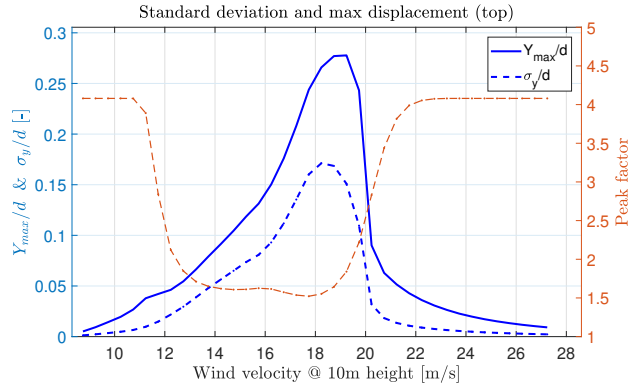


Figure 5.20: Standard deviation, peak factor and maximum displacement at the tower top (contour model)

A comparison of the resulting moments at the tower bottom are plotted versus the wind velocity at 10 m height and are presented in Figure 5.21.

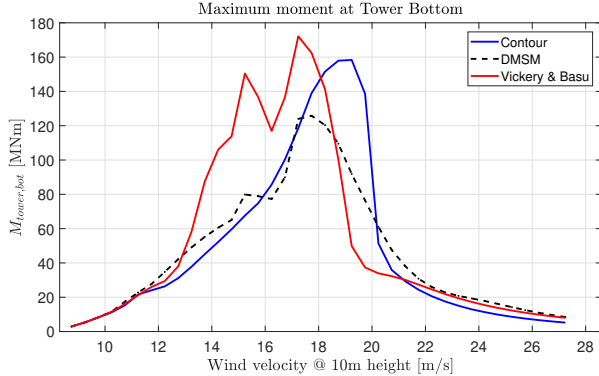


Figure 5.21: Bending moment at the tower bottom versus wind velocity

The “earlier” evolution of the phenomenon in V&B model can be explained from the higher values of aerodynamic parameter K_a , observed in Figure 4.6. Furthermore, despite the positive contribution of aerodynamic damping derived from the contour approach, the resulting vibration amplitude is higher than Lupi’s (DMSM) model.

5.2 Parametric study

In this section, a comparative study is performed for the selected different approaches followed by a sensitivity analysis of selected input parameters. The selected models are the three versions of the resonant models (see Chapter 3). Moreover, the second approach of the Eurocode is included which is a simplification of the V&B model. CICIND model code in 1999 proposed a similar model with the only exception of including the effect of turbulence intensity. Finally, the above presented models, meaning V&B, Lupi's and contour models are the main approaches of this sensitivity analysis, as parameters such as turbulence intensity I_v and shear exponent factor a can be considered.

In Figure 5.22, the vibration amplitudes computed from the resonant models are presented. In addition, in Figure 5.23, the amplitudes computed from the 2nd approach of the Eurocode and the CICIND model code (1999) are illustrated. It has to be mentioned that the maximum deflection from these models is derived from one wind velocity (one case) per damping value. This case refers to the critical wind velocity of the reference diameter. This is not exactly the case for the modified version of the resonant model, in which a variation of the critical velocity along tower height is considered. However, one case of vibration amplitude is also considered for this variation of critical velocities.

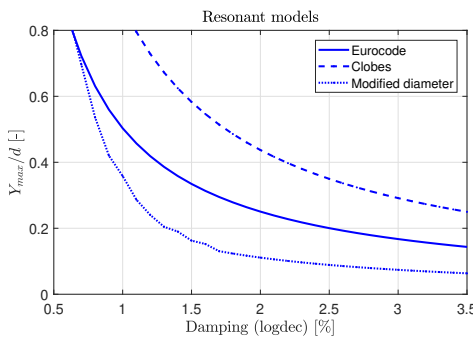


Figure 5.22: Y_{max}/d versus logdec of structural damping δ_s by resonant models

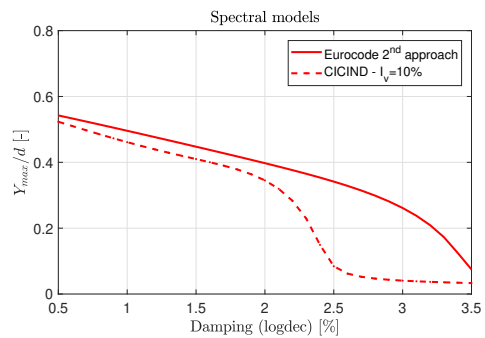


Figure 5.23: Y_{max}/d versus logdec of structural damping δ_s by spectral models

It can be observed that in the resonant models the self-limiting behavior of the phenomenon is absent. This indicates the simplicity of those models and the empirical derivation of their formulation based mainly on observed/measured amplitudes.

However, they have been used vastly the last decades for the prediction of the VIV response of towers and in many cases the results are matching the prediction. Regarding the second approach of the Eurocode and CICIND model, they are simplifications of the V&B approach and are presented here only for comparison reasons.

In the following Figure 5.24, the dependence of vibration amplitude on the structural damping of the three spectral models, which are presented extensively in Chapter 4, is illustrated. Two different values of turbulence intensity ($I_v = 1\%$ and $I_v = 10\%$) are considered indicating its effect on the resulting tower deflection.

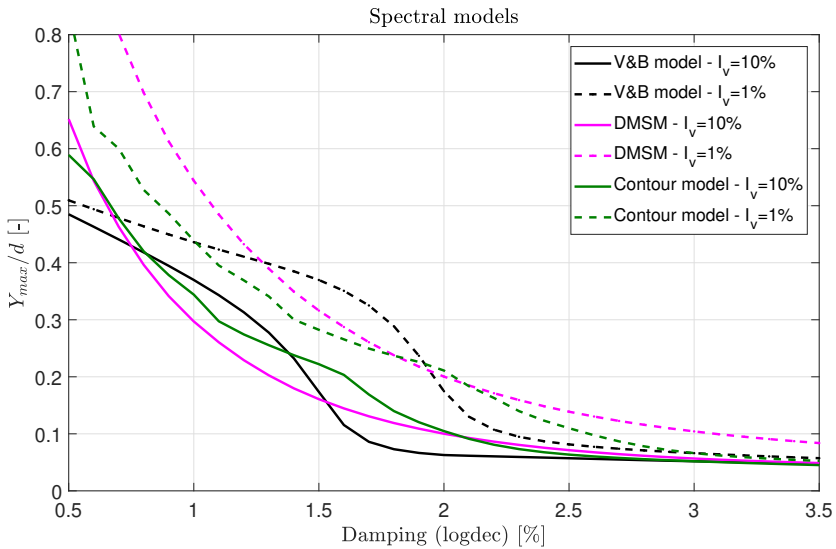


Figure 5.24: Normalized vibration amplitude versus logarithmic decrement of structural damping δ_s

The lower turbulence intensity results to higher vibration amplitudes as it is expected. For values of structural damping higher than 2%, the vibration response goes lower than 20% of the reference diameter. The self-limiting character of the phenomenon is illustrated by these models, as the response is limited to a certain value depending on the model. In addition, it can be observed in comparison with the curve obtained from the Ruscheweyh's model (see Figure 5.22), that DMSM of $I_v = 1\%$ is in a good agreement with Ruscheweyh's approach proposed in the Eurocode. It is an interesting result as the two models are based on completely dif-

ferent theoretical approaches. Therefore, since the so called DMSM model is based on experiments while Ruscheweyh's is mainly an empirical one, this similarity may validate Lupi's model behavior. Finally, the validation of the implementation of the models can also be observed in comparison with Figure 3.10.

In the next Figure 5.25, the effect of turbulence intensity on the amplitude of the vibration derived from the three spectral models is illustrated. The structural damping is set to the initial value of $\delta_s = 1.2\%$.

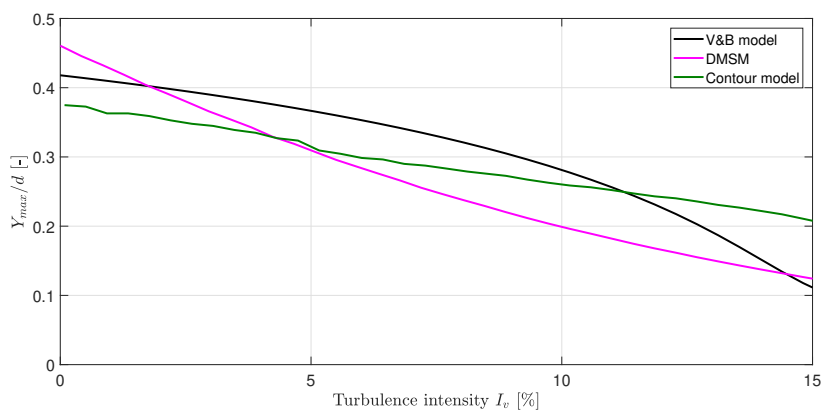


Figure 5.25: Normalized vibration amplitude versus turbulence intensity I_v

It can be immediately observed the importance of turbulence intensity as an input on these models. Even if the values of $I_v \leq 5\%$ may not be quite realistic, they were included for comparison reasons. It should be noted that no other model except for the CICIND one, considers the disruptive effect of turbulence. According to the second approach of the Eurocode, this effect is advised to be taken into account according to the national annexes.

Wind shear is quantified as the exponent a in the power law equation. Exponent a is another influencing parameter of the spectral models, as their formulation is presented in this thesis. It should be mentioned again that the formulation of those models by their researchers is not the same as in this thesis. Their implementation is done according to Verboom and van Koten publication [63]. In this way the shear of the wind profile is taken into account and its effect on the predicted responses is presented in Figure 5.26.

62 5. STUDY CASE OF VORTEX INDUCED VIBRATIONS ON WIND TURBINE TOWERS

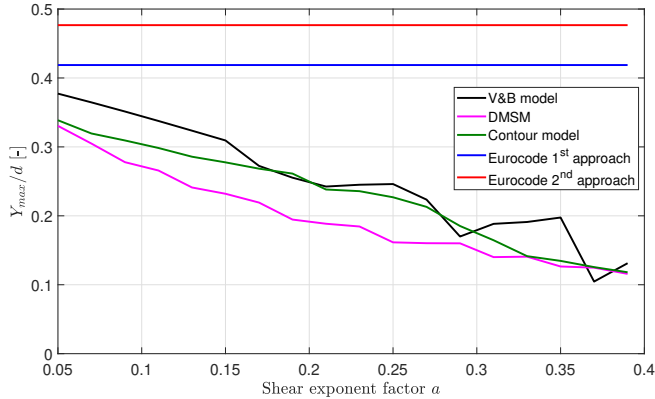


Figure 5.26: Normalized vibration amplitude versus shear exponent a

In the following Figure 5.27, the effect of air density ρ_{air} is considered. As presented by Clobes [13] (see Figure 3.11), the air density can either decrease or increase according to the air temperature. In combination with the fact that most of the extreme vibration amplitudes due to VIV have been observed during winter at night (low turbulence and higher air density), leads to include also ρ_{air} as an input parameter for the parametric study.

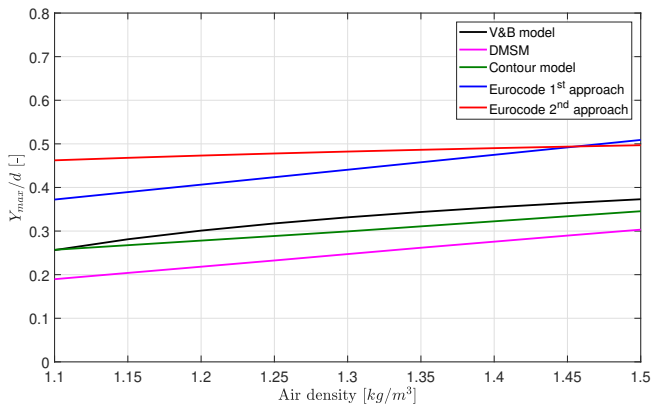


Figure 5.27: Normalized vibration amplitude versus air density ρ_{air}

It can be noticed the linearly dependence of the vibration amplitude with the increase of the air density. Only in the spectral approach of the Eurocode, this amplification effect is much lower. The rest of the models were not presented as they are directly related to the above presented models.

Finally, the last parameter that can be considered is the Strouhal number S_t . In the resonance models, where the lift force is directly related with the velocity squared V_{cr}^2 , the dependence on S_t is significant. Regarding the spectral models, as the aerodynamic parameter K_a is presented always versus the ratio V_m/V_{cr} , the effect of Strouhal number is limited to the magnitude of the lift force. However, the importance of the lift force is usually insignificant in the lock-in range. The computed normalized vibration amplitudes versus the Strouhal number are presented in Figure 5.28.

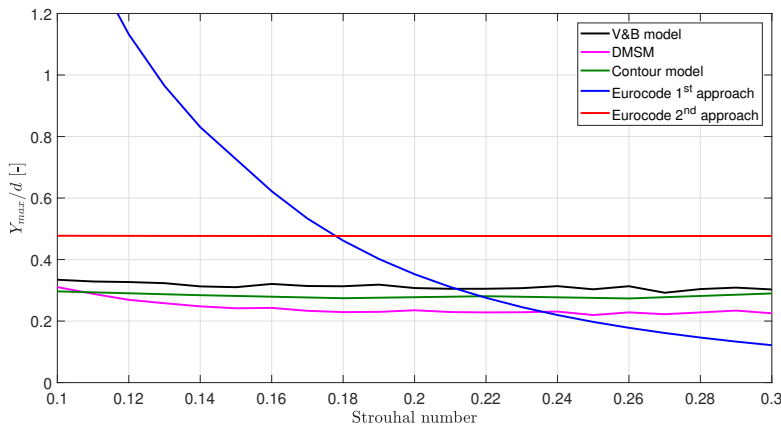


Figure 5.28: Normalized vibration amplitude versus Strouhal number S_t

However, the effect of Strouhal number is insignificant on the spectral models, when structural damping is low, and a driving input parameter for the resonant model. The same analysis performed for a value of structural damping equal to $\delta_s = 2\%$ instead of $\delta_s = 1.2\%$. The results are presented in Figure 5.29.

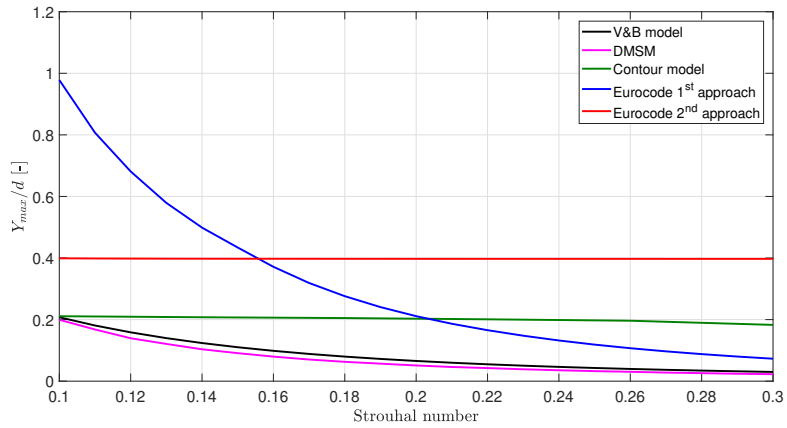


Figure 5.29: Normalized vibration amplitude versus Strouhal number S_t
($\delta_s = 2.0\%$)

Now the effect of the Strouhal number is more profound on DMSM and V&B model, as the total damping of the system does not get to values close to zero. Therefore, the modal lift force contributes more on the amplification of the vibration amplitude (see Figure 4.3).

In addition, Strouhal number is not expected to affect always the vibration amplitude but defines the velocity range in which VIV is expected. As it will be presented in Chapter 6, the range of wind velocities is crucial for the fatigue lifetime of the tower.

Chapter 6

Fatigue

In this Chapter the effect of vortex induced loading on the fatigue lifetime of the wind turbine tower is examined. The models which will be considered are the three spectral models as they are the only ones where the vibration amplitude of the towers is obtained over a range of wind velocities. The vortex induced load on the wind turbine towers is calculated in Chapter 5. According to this vortex load, fatigue assessment on the towers is performed assuming a probability density function (pdf) of the wind velocity.

6.1 Fatigue assessment

Vibrations on the wind turbine towers can be driving mechanism for the ULS design of the foundation frame or the sea fastening. This can also be the case for low damped structures. Except for the ULS, VIV events can be critical due to fatigue damage on the structures. Since the towers are subjected to repeated cyclic loading, developing of cracks can lead to structural failure. Numerous cases of industrial chimneys have been identified where repairs are necessary after VIV events. According to Eurocode, fatigue from cross-wind vortex vibrations normally governs chimney design. On the other hand, the wind turbine towers are designed for years of operation offshore, where VIV is insignificant due to the RNA mass, and any significant fatigue damage due to VIV onshore is unacceptable.

The considered spectral models presented extensively in Chapter 4, compute the standard deviation of the displacement σ_y as the solution is found in the frequency domain. VIV phenomenon can lead to a very large number of cycles of the same

stress range. In this Chapter, the case of the towers on the quay side will be examined. In this case, the time period is the biggest one and the risk of a serious VIV event is higher and can be more destructive. Therefore, in order to calculate the number of cycles for this specific period of time a Weibull distribution will be used. The probability of wind velocities in such a short period cannot be described accurately by a Weibull distribution, but for this study case seems sufficient to relate the number of oscillations with a statistical distribution of the wind velocity. More accurate and realistic analysis can be performed by using parameters fitted to measured wind velocities for the specific site and time of the year, considering in this way seasonal effects. Nevertheless, in this study case the Weibull distribution presented in Figure 6.1 will be used.

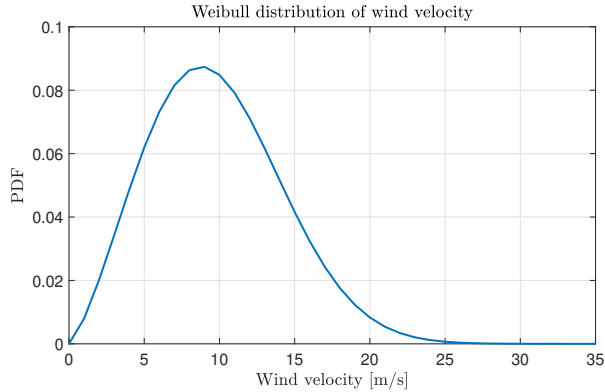


Figure 6.1: Probability density function of the wind velocity following a Weibull distribution

Afterwards, the stress ranges should be computed. The spectrum of the displacements has already been calculated in the implementation of the spectral models. It is presented in equation 6.1 for clarification reasons.

$$S_{uu}(z, \omega) = |H(z, \omega)|^2 \cdot S_{wv}(\omega) = |H(\omega) \cdot \Phi(z)|^2 \cdot S_{wv} \quad (6.1)$$

The variation of the displacements for this case is calculated by integrating the response spectrum over the frequency range (see equation 6.2).

$$\sigma_y^2 = \int_{-\infty}^{\infty} S_{uu}(z, \omega) d\omega \quad (6.2)$$

Consequently, the standard deviation of the bending moments $\sigma_M(z)$ along the height of the tower is computed. The next step is the calculation of the damage equivalent loads (DELs) which can be determined from the variance based on narrow band assumptions according to equation 6.3 [54].

$$\Delta M_{eq} = DEL = (8 \cdot m_0)^{0.5} \cdot \left[\Gamma \left(\frac{2+m}{2} \right) \right]^{1/m} \quad (6.3)$$

where m_0 is the zeroth spectral moment and Γ the gamma function. m is the inverse slope of the S-N curve. For steel structures two slopes are proposed of $m = 3$ and $m = 5$. However, it can be approximated with one slope of $m = 4$. Therefore, equation 6.3 transforms to equation 6.4.

$$\Delta M_{eq} = (8 \cdot m_0)^{0.5} \cdot \left[\Gamma \left(\frac{2+4}{2} \right) \right]^{1/4} = (8 \cdot m_0)^{0.5} \cdot 1.189 = 3.363 \cdot \sigma_M(z) \quad (6.4)$$

as $\sqrt{m_0}$ is the standard deviation of the bending moment. The total number of cycles of the structure is $N_{ref} = f_n \cdot T$, where T is the time duration in seconds. The so called 1 Hz DELs are defined as $N_{ref,1Hz} = T$. Therefore, the DEL is converted as presented in the following equation 6.5.

$$\Delta M_{eq,N_{ref}1Hz}(z) = 3.363 \cdot \sigma_M(z) \cdot \left(\frac{N_{ref}}{N_{ref,1Hz}} \right)^{1/m} = 3.363 \cdot \sigma_M(z) \cdot (f_n)^{0.25} \quad (6.5)$$

These equivalent moments have a frequency of 1 Hz and cause the same damage with the stochastic response of the system. The next step is the calculation of the bending stresses due to the damage equivalent moment $\Delta M_{eq,N_{ref}1Hz}(z)$ according to the well known equation 6.6.

$$\sigma_b(z) = \frac{\Delta M_{eq,N_{ref}1Hz}(z) \cdot d(z)}{2 \cdot I(z)} \quad (6.6)$$

The vibration amplitudes σ_y considered from the three spectral models (V&B, DMSM, Contour) in this case are presented in Figure 6.2.

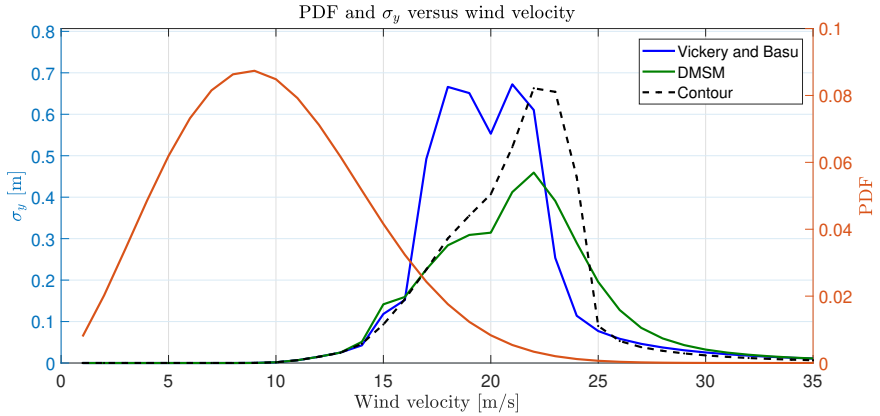


Figure 6.2: Standard deviation of the displacement σ_y and pdf versus wind velocity

One can observe the probabilities of the different responses derived from the models and qualitatively get an indication of the fatigue damage on the structure. Afterwards, the bending stresses along tower considering the stress concentration factors for each cross section are presented in Figure 6.3. The maximum vibration case is considered even if the probability of this wind velocity is very low.

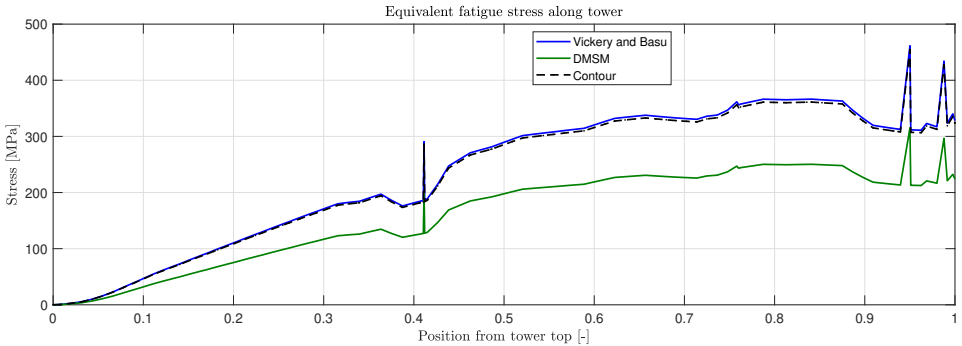


Figure 6.3: Equivalent fatigue bending stresses along tower for maximum vibration amplitude

Since the σ_y computed from V&B and the contour model are almost the same, the equivalent bending stresses are at almost the same level. However, the maximum

deflection is found at different wind velocities affecting in this way the accumulating fatigue damage on the tower.

Assuming a total duration of one day ($T = 86400$ sec) on the quay side, according to the pdf considered, the total number of seconds per wind velocity can be computed. In this way, multiplying the number of seconds with the stress range of each wind velocity, the DEL for each case can be calculated. A material safety factor for fatigue is also taken into account. Following, the number of cycles to failure for each stress range are computed based on the detail category $\sigma_c(z)$ of each section. Moreover, the constant amplitude fatigue limit is computed $(\frac{2}{5})^{1/3} \cdot \sigma_c(z)$. Knowing the oscillations per stress range and the maximum ones to failure, fatigue damage for each wind velocity can be computed. The total damage D_{tot} can be derived by using the Palmger-Miner rule (see equation 6.7).

$$D_{tot} = \sum_{i=1}^{n_{tot}} \frac{n_i}{N_i} \tag{6.7}$$

In the following Figure 6.4, the predicted fatigue damage per cross section for a duration of one day is presented for the three models.

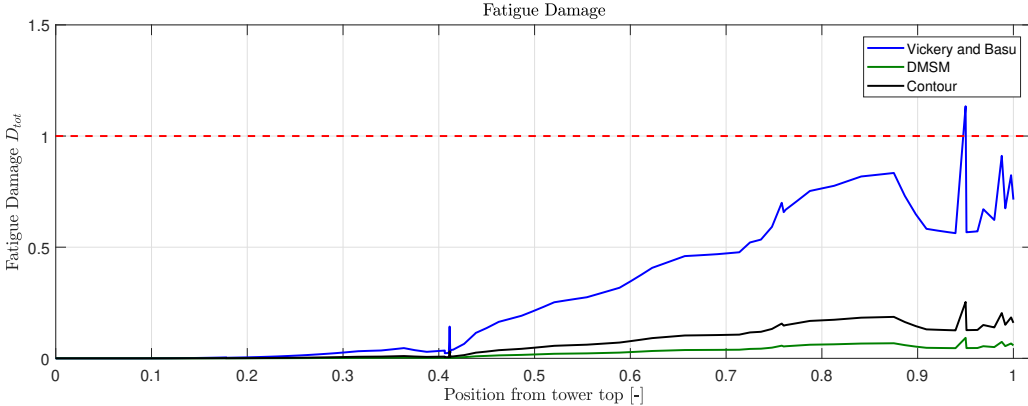


Figure 6.4: Fatigue bending stresses along tower for maximum vibration amplitude

One can observe the severity of the phenomenon and its effect on the fatigue lifetime of the tower. In less than a day one cross section, according to the deflection computed by V&B model, fails due to VIV. Furthermore, even if the vibration amplitudes of contour and V&B models are similar, due to the probabilities of the

wind velocities, different fatigue damage is computed. Finally, the fatigue lifetime for each cross section based on the three models is presented in Figure 6.5.

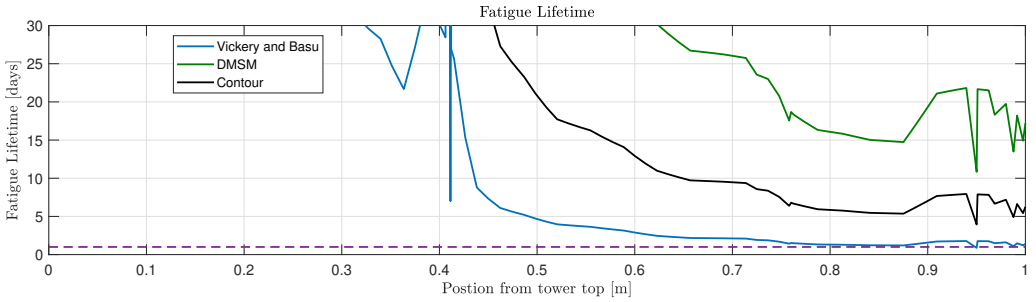


Figure 6.5: Fatigue lifetime for each cross section along the tower

It can be observed that the previously mentioned cross section close to the tower bottom fails due to fatigue damage in less than a day. This results from the V&B model which is, in this case, the most conservative one. Regarding the other two models, none of the cross sections fail for this specific, very limited time duration (one day). Finally, for the cross section close to the tower bottom, the S-N curve, the equivalent fatigue stress ranges and the cumulative fatigue damage are presented in Figure 6.6 as derived by V&B model.

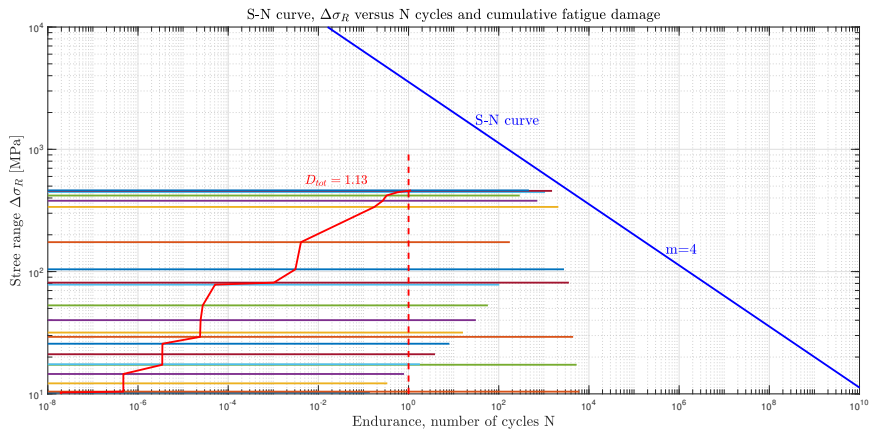


Figure 6.6: S-N curve and fatigue accumulation damage for the most critical section

In accordance with the previous Chapter 5, the importance of the Strouhal number is now more profound. Strouhal number S_t , as shown in the sensitivity analysis is not affecting the vibration amplitude of the spectral models significantly. However, it defines the range of wind velocities at which VIV is occurring. Therefore, considering the probability of the wind velocity of a specific site one can estimate the susceptibility of the towers to VIV events. Undoubtedly, the level of uncertainty regarding the wind velocities complicates significantly the accurate prediction of tower's fatigue damage.

Afterwards, for comparison reasons, the same case is computed considering $\delta_s = 2.0\%$ instead of $\delta_s = 1.2\%$ logdec. The vibration amplitudes are much lower as can be seen in Figure 6.7.

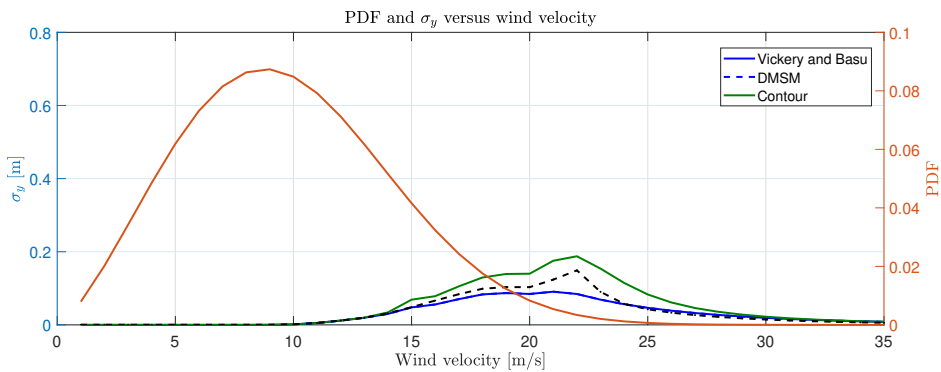


Figure 6.7: Standard deviation of the displacement σ_y for $\delta_s = 2\%$ and pdf versus wind velocity

Considering these lower amplitudes, the fatigue lifetime of the tower is increasing significantly. The equivalent bending stresses are six times lower and the fatigue damage is at least 2000 times lower for the same time duration. The resulting fatigue lifetime is presented in Figure 6.8.

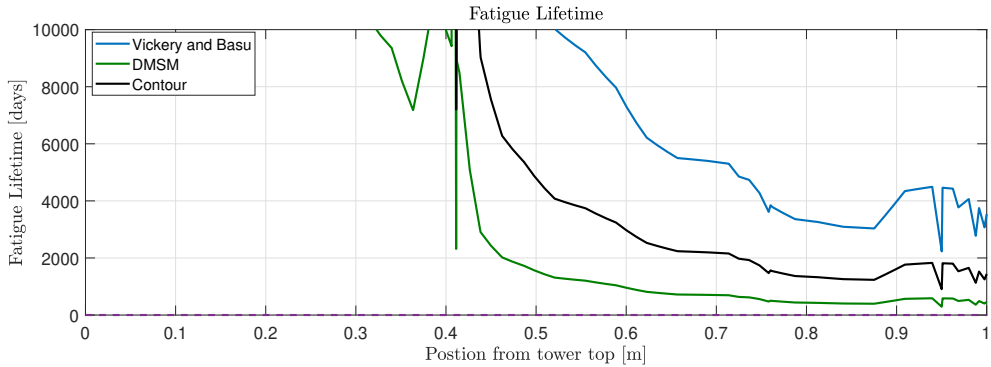


Figure 6.8: Fatigue lifetime for each cross section along the tower

Concluding, fatigue damage on the wind turbine towers can be extremely high for low damped structures. Accurate estimation of the tower damping is necessary for the design. Installation of damper systems can be a solution if damping is found to be insufficient.

Chapter 7

Conclusions

In this study, an investigation of the VIV phenomenon regarding the wind turbine towers was performed. Various models proposed by the standards and the literature were examined. The thesis objective was to gain a deeper understanding on this complex phenomenon and through the analysis of the existing methods develop a more realistic, trustworthy and reliable model for the prediction of the response of wind turbine towers. The tapered section at the top of these structures complicate the accurate solution of the problem.

7.1 Conclusions

The main conclusions that can be made from this study are the following:

- An extensive literature review was performed and presented in this thesis. Main researchers were identified and their models were explained, commented and presented in the previous Chapters. A brief explanation of the nature of the phenomenon and the main experimental techniques were presented in Chapter 2. A deeper knowledge and understanding of VIV nature was achieved, contributing to the critical review of the existing calculation methods.
- Existing models proposed by the Standards (e.g. Eurocode 1st and 2nd approach) are simplified versions of original ones presented in the literature. These calculation methods, taking into account the tapered section of the tower, can be considered only for comparative studies and quick computations. The Effective Correlation Method presented in Chapter 3 is based on

experimental evidences regarding the increase of correlation length with increasing amplitude. However, the model is an empirical one adjusted to observed or measured vibration amplitudes of towers due to VIV. Therefore, only the version considering the tapered section of the structure, which is in a good agreement with DMSM can be considered. Regarding the 2nd approach of the Eurocode, simplifications made on V&B model do not allow acquisition of better insight and intuition of the computed amplitudes.

- The main focus of this research was on the spectral models, V&B, DMSM and the proposed contour approach. A model implementing the dependence of the vibration amplitude on the wind characteristics (wind velocity, profile, turbulence intensity) and the variation of the diameter along the tower is proposed. In addition, data from Lupi's experiments were processed and the contour approach was developed. The contour model is regarded as more reliable than the other approaches, representing the physics of the VIV phenomenon as it was derived directly from experimental results.
- Sensitivity analysis shows that the most influencing input parameter is the structural damping of the wind turbine tower. Above a certain value of ζ_s the vibration amplitudes decreases significantly, minimizing the potential damage due to VIV. Furthermore, wind shear factor a affects a lot the resulting amplitudes, illustrating the impact of the wind profile. Strouhal number S_t changes the critical wind velocities V_{cr} affecting only the amplitude derived from the resonant model. Spectral models, as they consider the dependence of the negative damping parameter K_a on the critical wind velocity V_{cr} , are not significantly affected by the change of Strouhal number.
- Fatigue assessment on the towers due to VIV shown the severity of the phenomenon on low damped structures. In these cases, either additional damping devices (TMD or TLD) should be considered or suppression measures such as helical strakes should be applied.

In conclusion, the contour model adds value to the models that are present today. The different process of the results derived from forced oscillation experiments conducted in air, including the dependence of forced coefficients (in this case the aerodynamic parameter K_a) on the V_m/V_{cr} ratio is introduced, developed and implemented in this research. The necessity of calculating the vibration amplitude versus the wind velocity was the driving factor for the development of that approach. Moreover, more realistic calculations of the fatigue damage can be derived due to the amplitude dependency on the wind velocity, as presented in Chapter 6. The

solution is “found” in the frequency domain, achieving “quick” results and can be implemented on various tower geometries or other cylindrical structures.

7.2 Recommendations for future work

The developed contour model should be further validated and can be modified for the prediction of the towers response due to VIV in more complex cases. The following recommendations are made for the developed spectral model:

- The model should be validated with measured/observed vibration amplitudes of the wind turbine towers. This requires measurement data not only for the amplitude of the vibration, but also the wind velocity, direction and the turbulence intensity of the specific event. In addition, structural properties of the tower should be adequately defined (especially structural damping ζ_s) for the proper validation of the developed model. Simulations performed in the time domain in comparison with measured time series will contribute to the understanding and explanation of the VIV development on the towers.
- Simulations performed in a CFD software can validate/modify the experimental values for the force coefficients which were measured at low Reynolds number. Comparison of the simulated (CFD) aerodynamic parameter K_a with the measured one (experiments) would be very interesting, especially in areas of very low or very high amplitudes where wind tunnel tests cannot sufficiently reproduce. In addition, three dimensional simulations should be performed in order to examine the force correlation along the height of the tower, the effect of changing the wind direction (separation points) and the effect of turbulence intensity I_v .
- In the case of tower arrangements in groups, amplification of the force coefficients (increase of K_a) is expected. Furthermore, effectiveness of strakes application over the top third of the tower as a mitigation measure is another uncertainty. Therefore, experimental studies should be conducted investigating the “group” and the strakes effect on the negative aerodynamic parameter K_a . Different cylinder arrangements with various distances should be included in order to derive reliable results, applicable to different cases. In this way, the model will be capable of more accurate prediction of the vibration amplitude in those cases.
- Finally, Vortex Induced Vibration is a very interesting phenomenon whose complexity depends on various parameters. Future work can focus a lot of different

cases of VIV. For example, effect of wall proximity, near end effects, variation of Strouhal number along the height of a tapered cylinder, effectiveness of mitigation measures on suppression of VIV phenomena are only some areas of potential future research.

Appendix A

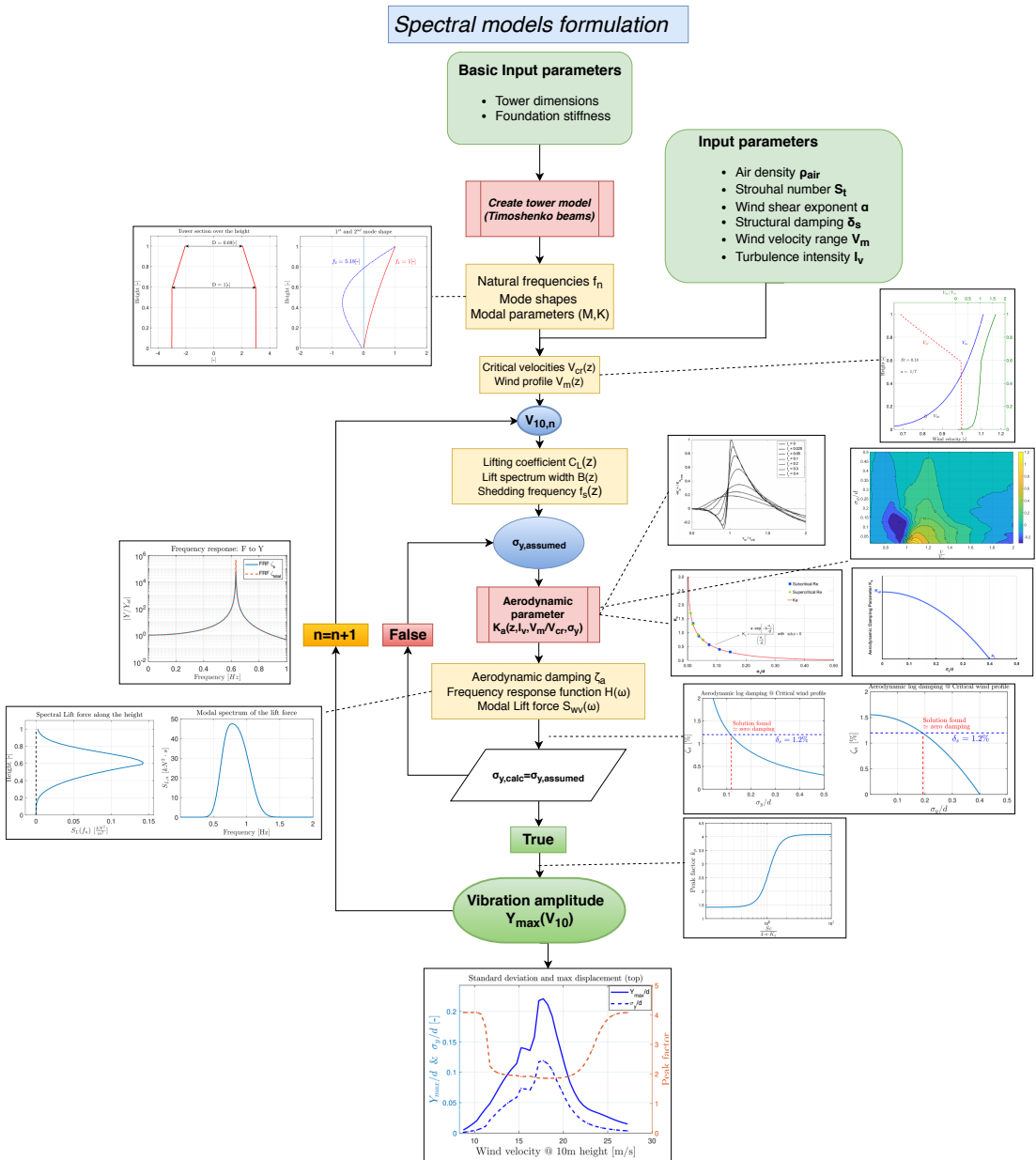


Figure A.1: Flowchart of the spectral models implementation

Bibliography

- [1] www.wikiwand.com
- [2] www.multitech-fr.com
- [3] www.engineeringtoolbox.com
- [4] *Eurocode 1: Actions on Structures, Part 1-4: General Actions - Wind Actions*. 2010.
- [5] R. E. D. Bishop. The lift and drag forces on a circular cylinder oscillating in a flowing fluid. *Proceedings of the Royal Society of London A: Mathematical, Physical and Engineering Sciences*, 277(1368):51–75, 1964.
- [6] R. I. Basu and B. J. Vickery. Across-wind vibrations of structure of circular cross-section. Part II. Development of a mathematical model for full-scale application. *Journal of Wind Engineering and Industrial Aerodynamics*, 12(1):75–97, 1983.
- [7] Roger Indranath Basu. *Across-wind Response Of Slender Structures Of Circular Cross-section To Atmospheric Turbulence*. 1983.
- [8] Richard Evelyn Donohue Bishop and AY Hassan. The lift and drag forces on a circular cylinder in a flowing fluid. *Proc. R. Soc. Lond. A*, 277(1368):32–50, 1964.
- [9] Robert Blevins. *Flow-Induced Vibration*, 2001.
- [10] J. Carberry, J. Sheridan, and D. Rockwell. Controlled oscillations of a cylinder: Forces and wake modes. *Journal of Fluid Mechanics*, 538:31–69, 2005.

- [11] J. C.K. Cheung and W. H. Melbourne. Turbulence effects on some aerodynamic parameters of a circular cylinder at supercritical numbers. *Journal of Wind Engineering and Industrial Aerodynamics*, 14(1-3):399–410, 1983.
- [12] J.C.K CHEUNG and W.H.MELBOURNE. Aerodynamic damping of a circular cylinder in turbelent flow at high Reynolds numbers. pages 5–8. Eighth Australian Fluid Mechanics Conference, 1983.
- [13] Mathias Globes, Andreas Willecke, and Udo Peil. Vortex excitation of steel chimneys : Two ultimate limit states. (1986):2–9, 2005.
- [14] Ray W Clough, Joseph Penzien, and DS Griffin. Dynamics of structures. *Journal of Applied Mechanics*, 44:366, 1977.
- [15] M E Davies. A comparison of the wake structure of a stationary and oscillating bluff body, using a conditional averaging technique. *Journal of Fluid Mechanics*, 75:209–231, 1976.
- [16] Hiroshi Tanaka DrEng. Pressure correlations on a vibrating cylinder. In *Proceedings of the Fourth International Conference on Wind Effects on Buildings and Structures: Heathrow 1975*. Cambridge University Press, 1977.
- [17] Claes Dyrbye and Svend Ole Hansen. *Wind Loads on Structures*. John Wiley and Sons, 1996.
- [18] S E. Ramberg and O M. Griffin. Vortex formation in the wake of a vibrating, flexible cable. 96:317, 12 1974.
- [19] C. C. Feng. The measurement of vortex induced effects in flow past stationary and oscillating circular and D-section cylinders. *Retrospective Theses and Dissertations, 1919-2007*, (October):100, 1963.
- [20] CC Feng. *The measurement of vortex induced effects in flow past stationary and oscillating circular and d-section cylinders*. PhD thesis, University of British Columbia, 1968.
- [21] By Indranil Goswami. CYLINDERS . I : . 119(11):2270–2287, 1994.
- [22] By Indranil Goswami, Robert H Scanlan, and Nicholas P Jones. V O R T E X - I N D U C E D V I B R A T I O N O F C I R C U L A R C Y L I N D E R S . II : N E W M O D E L boundary conditions . Such a solution remains elusive to date . Furthermore , in spite of the phenomenal increase in computational resources in recent times . 119(11):2288–2302, 1994.

- [23] R. N. Govardhan and C. H.K. Williamson. *Defining the 'modified Griffin plot' in vortex-induced vibration: Revealing the effect of Reynolds number using controlled damping*, volume 561. 2006.
- [24] Owen M. Griffin and Steven E. Ramberg. The vortex-street wakes of vibrating cylinders. *Journal of Fluid Mechanics*, 66(3):553–576, 1974.
- [25] Svend Ole Hansen. Vortex-induced vibrations - the Scruton number revisited. *Proceedings of the Institution of Civil Engineers - Structures and Buildings*, 166(10):560–571, 2013.
- [26] G Hirsch and H Ruscheweyh. Full-Scale Measurements on steel chimney stacks. *Journal of Industrial Aerodynamics*, 1:341–347, 1975.
- [27] F. S. Hover, A. H. Techet, and M. S. Triantafyllou. Forces on oscillating uniform and tapered cylinders in crossflow. *Journal of Fluid Mechanics*, 363:97–114, 1998.
- [28] Asif Khalak and Charles H.K. Williamson. Investigation of relative effects of mass and damping in vortex-induced vibration of a circular cylinder. *Journal of Wind Engineering and Industrial Aerodynamics*, 69-71:341–350, 1997.
- [29] John H. Lienhard. Synopsis of lift, drag, and vortex frequency data for rigid circular cylinders, 1966.
- [30] Francesca Lupi, Hans Jürgen Niemann, and Rüdiger Höffer. A novel spectral method for cross-wind vibrations: Application to 27 full-scale chimneys. *Journal of Wind Engineering and Industrial Aerodynamics*, 171(October):353–365, 2017.
- [31] Francesca Lupi, Hans Jürgen Niemann, and Rüdiger Höffer. A novel spectral method for cross-wind vibrations: Application to 27 full-scale chimneys. *Journal of Wind Engineering and Industrial Aerodynamics*, 171(May):353–365, 2017.
- [32] Francesca Lupi, Hans Jürgen Niemann, and Rüdiger Höffer. Limit Cycles in Vortex-Induced Vibrations: A Critical Analysis. *Procedia Engineering*, 199:699–704, 2017.
- [33] Francesca Lupi, Hans Jürgen Niemann, and Rüdiger Höffer. Aerodynamic damping model in vortex-induced vibrations for wind engineering applications. *Journal of Wind Engineering and Industrial Aerodynamics*, 174(January):281–295, 2018.

- [34] AW Marris. A review on vortex streets, periodic wakes, and induced vibration phenomena. *Journal of Basic Engineering*, 86(2):185–193, 1964.
- [35] TL Morse and CHK Williamson. Prediction of vortex-induced vibration response by employing controlled motion. *Journal of Fluid Mechanics*, 634:5–39, 2009.
- [36] M Novak and H Tanaka. Pressure correlations on a vibrating cylinder. pages 227–232, 01 1975.
- [37] A. Ongoren and D. Rockwell. Flow structure from an oscillating cylinder part1. *Journal of Fluid Mechanics*, 191:225 – 245, 1988.
- [38] Christian Petersen. *Dynamik der Baukonstruktionen*. Springer-Verlag, 2013.
- [39] H Ruscheweyh. Tip effect on vortex-excited oscillation of a model stack of cantilevered cylinders with and without efflux stream. In *IUTAM-Symp. on Flow-Induced Structural Vibrations, Karlsruhe, 1972*.
- [40] H Ruscheweyh. Dynamische windwirkung an bauwerken. band 1. grundlagen. band 2. praktische anwendungen. 1982.
- [41] H. Ruscheweyh. Problems with in-line stacks: Experience with full-scale objects. *Engineering Structures*, 6(4):340–343, 1984.
- [42] H. Ruscheweyh. Vortex-excited vibrations of yawed cantilevered circular cylinders with different scruton numbers. *Journal of Wind Engineering and Industrial Aerodynamics*, 23(C):419–426, 1986.
- [43] H Ruscheweyh. Codification of vortex excited vibrations. recent advances in wind engineering. In *Proceedings of the 2nd Asia-Pacific Symposium on Wind Engineerig., Beijing, China, Int. Acad. Publ., Pergamon Press*, volume 1, pages 362–72, 1989.
- [44] H. Ruscheweyh. Practical experiences with wind-induced vibrations. *Journal of Wind Engineering and Industrial Aerodynamics*, 33(1-2):211–218, 1990.
- [45] H. Ruscheweyh and B. Dielen. Interference galloping-investigations concerning the phase lag of the flow switching. *Journal of Wind Engineering and Industrial Aerodynamics*, 43(1-3):2047–2056, 1992.
- [46] H. Ruscheweyh and G. Sedlacek. Crosswind vibrations of steel stacks. - critical comparison between some recently proposed codes -. *Journal of Wind Engineering and Industrial Aerodynamics*, 30(1-3):173–183, 1988.

- [47] T. Sarpkaya. A critical review of the intrinsic nature of vortex-induced vibrations. *Journal of Fluids and Structures*, 19(4):389–447, 2004.
- [48] Turgot Sarpkaya. Fluid forces on oscillating cylinders. *NASA STI/Recon Technical Report A*, 78:275–290, 1978.
- [49] Neil Schlager. When technology fails: Significant technological disasters, accidents, and failures of the twentieth century. 1994.
- [50] C. SCRUTON. On the wind excited oscillations of stacks, towers and masts. *Proc. int. Conf. Wind Effects on Build. and Struct., Her Majesty's Stationary Office*, 298, 1963.
- [51] C Scruton. *On the wind-excited oscillations of stacks, towers and masts*. Teddington, Middlesex, 1963. Paper 16 to be presented at the International Conference on the Wind Effects on Buildings and structures, 1963.
- [52] C SCRUTON and A R FLINT. Wind-Excited Oscillations of Structures. *Proceedings of the Institution of Civil Engineers*, 27(4):673–702, 1964.
- [53] Ch Scruton. A means for avoiding wind-excited oscillations of structures with circular or nearly circular cross section. *Natl. Phys. Lab.(UK), Aero Rep.*, 1957.
- [54] Marc Seidel. Wave induced fatigue loads: Insights from frequency domain calculations. *Stahlbau*, 83(8):535–541, 2014.
- [55] V. Strouhal. Ueber eine besondere Art der Tonerregung. *Annalen der Physik*, 241(10):216–251, 1878.
- [56] Roland B Stull. *An introduction to boundary layer meteorology*, volume 13. Springer Science & Business Media, 2012.
- [57] B.M. Sumer. Chapter 1: Flow around a cylinder in steady current. *Hydrodynamics Around Cylindrical Structures*, page 1, 2006.
- [58] FredsÅ,e JÃ,rge Sumer, B. Mutlu. World Scientific, 2006.
- [59] Y TANIDA, A OKAJIMA, and Y WATANABE. STABILITY OF A CIRCULAR CYLINDER OSCILLATING IN UNIFORM FLOW OR IN A WAKE. *Journal of Fluid Mechanics*, 61(4), 1973.
- [60] G. H. Toebes. The Unsteady Flow and Wake Near an Oscillating Cylinder. *Journal of Basic Engineering*, 91(3):493, 1969.

- [61] GH Toebes. Fluidelastic features of flow around cylinders. In *Proceedings of the International Research Seminar, Wind Effects on Buildings and Structures*, pages 323–341, 1967.
- [62] H Van Koten. Wind load on chimneys. In *Proc. IASS Symposium on Industrial Chimneys, Krakow, Poland*, 1973.
- [63] G. K. Verboom and H. van Koten. Vortex excitation: Three design rules tested on 13 industrial chimneys. *Journal of Wind Engineering and Industrial Aerodynamics*, 98(3):145–154, 2010.
- [64] B. J. Vickery and R. Basu. Simplified approaches to the evaluation of the across-wind response of chimneys. *Journal of Wind Engineering and Industrial Aerodynamics*, 14(1-3):153–166, 1983.
- [65] B. J. Vickery and R. I. Basu. Across-wind vibrations of structures of circular cross-section. Part I. Development of a mathematical model for two-dimensional conditions. *Journal of Wind Engineering and Industrial Aerodynamics*, 12(1):49–73, 1983.
- [66] Barry J. Vickery. Across-wind buffeting in a group of four in-line model chimneys. *Journal of Wind Engineering and Industrial Aerodynamics*, 8(1-2):177–193, 1981.
- [67] Barry J. Vickery and Arthur W. Clark. Lift or across-wind response of tapered stacks, 1972.
- [68] R.D Vickery, B.J., Watkins. Flow-induced vibration of cylindrical structures, 1962.
- [69] Théodore Von Karman. Uber den mechanismus des flussigkeits-und luftwiderstandes. *Phys. Z.*, pages 49–59, 1912.
- [70] C. H.K. Williamson and R. Govardhan. A brief review of recent results in vortex-induced vibrations. *Journal of Wind Engineering and Industrial Aerodynamics*, 96(6-7):713–735, 2008.
- [71] C. H.K. Williamson and A. Roshko. Vortex formation in the wake of an oscillating cylinder. *Journal of Fluids and Structures*, 2(4):355–381, 1988.
- [72] Yi Yang. *Experimental Investigations of Vortex Induced Vibration of A Flat Plate in Pitch Oscillation*. PhD thesis, 2012.

-
- [73] M. M. Zdravkovich. Review and classification of various aerodynamic and hydrodynamic means for suppressing vortex shedding. *Journal of Wind Engineering and Industrial Aerodynamics*, 7(2):145–189, 1981.

